Mechanical Systems and Signal Processing 158 (2021) 107667

Contents lists available at ScienceDirect

Mechanical Systems and Signal Processing

journal homepage: www.elsevier.com/locate/ymssp

Drive-by methodology to identify resonant bridges using track irregularity measured by high-speed trains

Kodai Matsuoka [a,*], Hirofumi Tanaka [b], Kyohei Kawasaki [a], Claudio Somaschini [b], Andrea Collina [b]

[a] Railway Technical Research Institute, Railway Dynamics Division, 2-8-38, Hikari-cho, Kokubunji-shi, Tokyo 185-8540, Japan
[b] Politecnico di Milano, Department of Mechanical Engineering, Via G. La Masa 1, 20152 Milano, Italy

ARTICLE INFO

Article history:
Received 24 February 2020
Received in revised form 14 December 2020
Accepted 16 January 2021
Available online 6 March 2021

Keywords:
Drive-by system
Resonant bridge
High-speed railway
Rail irregularity

ABSTRACT

Resonance of railway bridges is a matter of major concern in high-speed railways because it reduces riding comfort, damages the attached structures, and decreases the strength of girder bodies. Although this abnormal behavior can be inspected using *in situ* displacement measurements taken from the ground, its investigation is tedious and, consequently, is very expensive. In this study, authors developed a novel drive-by system for high-speed railways to detect resonant bridges; the difference between two track irregularities at the same position using devices mounted on the first and last vehicles of a train was measured. This is based on the idea that the response of the last vehicle passing through the resonant bridge is attributed to the superposition of track irregularities and abnormal bridge displacement because of resonance mechanisms. However, the response of the first vehicle primarily arises from track irregularities since the resonance phenomenon is not yet sufficiently excited. The Resonance Detection Index (RDI), defined as the difference between the track irregularities measured by the devices mounted on the first and last vehicles, is used to emphasize the component excited by vehicle length to propose a methodology for detecting resonant bridges.

Numerical simulations clarify that bridge span and track irregularity have greater effects on the RDI than either measurement noise or positioning error. Track irregularity may cause the RDI to vary by ± 2 mm depending on vehicle length wave component of the track irregularity. Consequently, this study demonstrates that resonant bridges with spans between 20 and 60 m can be detected using the proposed RDI.

Finally, the proposed method was applied to track irregularity measurements using actual high-speed trains operating in Japan. More than ten bridges, out of more than 800 bridges, were detected as resonant bridges according to RDI. *In situ* displacement measurements were performed for three of these bridges, demonstrating the presence of resonance phenomenon and thereby validating the proposed method.

Abbreviations: RDI, Resonance detection index; SHM, Structural health monitoring.

* Corresponding author.
E-mail addresses: matsuoka.kodai.13@rtri.or.jp (K. Matsuoka), tanaka.hirofumi.96@rtri.or.jp (H. Tanaka), kawasaki.kyohei.96@rtri.or.jp (K. Kawasaki), claudio.somaschini@polimi.it (C. Somaschini), andrea.collina@polimi.it (A. Collina).

https://doi.org/10.1016/j.ymssp.2021.107667
0888-3270/

1. Introduction

In Japan, numerous high-speed railway structures, such as railway bridges, have been previously constructed. Human and economic resources for maintaining these structures are decreasing. Damage because of aging is becoming obvious in these structures [1]. Therefore, it has become crucial to develop a method for efficiently managing these aging structures and to ensure compliance to safety standards. A problem that has emerged in recent high-speed railways in Japan is the occurrence of large-amplitude vibrations in concrete railway bridges because of resonance phenomena [2,3]. Certain simply-supported concrete bridges that were built in large numbers on Japan's high-speed railways in the past suddenly started to resonate after decades of operation [2–4]. The number of resonances in the same type of bridges has been increasing [5]. The practical problems caused by resonance have been observed in other countries. In France, a case has been reported of a large-amplitude vibration because of resonance causing ballast destabilization in high-speed railways [6]. Bridges with significantly large dynamic responses caused by resonance could create serious troubles such as a decrease in the ride comfort, ballast instability, train operational problems (because of low-speed limit), and damage to catenaries via electric poles built on bridges [2,4–7]. Therefore, when large-amplitude bridge vibrations occur because of resonance, rapid detection, and countermeasures are required. However, it is not easy to inspect a very large number of high-speed railway bridges. In recent years, the introduction of condition-based maintenance by monitoring and vibration measurement has been studied because of the low cost of sensor systems and development of information and communications technology [8–12]. Even with these contributions, enormous human and economic resources are still required to deploy measurement equipment for entire routes. Therefore, comprehensive monitoring of the resonance state of all bridges is not currently feasible. An efficient and comprehensive way of inspecting a large number of railway bridges with a single run is the drive-by estimation of passing railway bridges based on the on-board measured data of a *in-service* train traveling on the specific routes [13,14]. Furthermore, high-frequency inspection can be realized by daily traveling; therefore, the drive-by resonant bridge evaluation would be an innovative system for providing resonant bridge detection and monitoring and for reducing the risks associated with resonant bridges. However, there are not sufficient studies on drive-by bridges inspection methods in high-speed railways [13]. In this study, a drive-by resonant bridge detection in high-speed railways is realized by a novel detection method using track irregularity data obtained from the first and last vehicles of a high-speed service train.

There are numerous studies on bridge performance evaluation and damage detection using the data measured from traveling vehicles. Drive-by bridge evaluation has been proposed for cost-effective structural health monitoring (SHM) [13,14]. SHM using sensors directly installed on structures are given in [8–12]. The theoretical and experimental feasibility studies for the bridge condition estimation using traveling vehicles have already been reported by Yang et al. [15] and Lin and Yang [16]. These authors subsequently presented the factors that influence drive-by bridge evaluation [17] and proposed the filtering approach to extract the response of the passing bridge, which is mixed with the on-board response [18]. Recently, Yang et al. [19] summarized drive-by bridge evaluation (termed vehicle scanning in [19]) and the applications of this technique to highway bridges and railway tracks were reviewed. In addition to these pioneering contributions, bridge vibration estimation by the drive-by system has been studied worldwide with focus on scaled model experiments [20–24]. In recent years, numerous drive-by bridge inspection methods have been proposed; these include methods that use a particle filter [25], a neural network [26], frequency-independent underdamped pinning stochastic resonance [27], the bridge displacement profile [28], and the bridge frequency with two vehicles [29]. In most of these studies and in SHM, the bridge fundamental frequency was indirectly identified by the frequency domain analysis of the mixed bridge responses of vehicles. However, Hester and Gonzales [13] stated in their review article on drive-by bridge inspection that bridge frequency identification using a drive-by system has been limited to relatively slow-moving vehicle in which vehicles stay for a long time on the bridges because of limited frequency resolution and bridge–vehicle interactions. When the vehicle travels at a high speed, the frequency resolution of the on-vehicle measured data and the transmission of the bridge response to the vehicle via the bridge–vehicle interactions are strictly limited. The measured vehicle response is used not only for the bridge frequency estimation but also for the evaluation and monitoring of the bridge damping [22,30–32] and the mode shape [33]. Furthermore, the response is used for measuring the static mechanical properties of bridges [23,34]. The detection of local damage in bridges has been primarily studied by numerical calculation by Nguyan and Tran [35], Zhang et al. [36], and Hester and Gonzales [13]. These studies have shown that the position and extent of damages that can be identified are greatly affected by the road profile, which does not include the bridge displacement, the vehicle travel speed, and the measurement noise.

Most studies have focused on road bridges. In the railways field, the developments of track irregularity estimation methods using traveling vehicles have been studied [37–44]. Methods for evaluating track irregularities by inertial measurements [41,45] have been introduced in certain service vehicles in Japan. However, a few examples focused on the railway bridges located under the track based on the data obtained from railway vehicles [46,47]. Matsuoka et al. [48] proposed a method for extracting bridge vibration components using short-time Fourier transform of the axle acceleration of a railway vehicle during low-speed running; they confirmed the method on a full-scale test line. Carnevale et al. [49] proposed a bridge local damage detection method using the bogie acceleration of a passing train and confirmed the applicability of the method up to 140 km/h using numerical simulations. Recently, Somaschini et al. [50] attempted to construct a drive-by bridge response extraction method that focused on the bogie responses for high-speed railways. Hester and Gonzales [13] indicated that there is limited research on a method for dealing with the maximum train speed of the current high-speed railway that

passes via the bridge in an instant. In another study, researchers noted that, unlike in a road bridge, multiple vehicles with regularly arranged axles pass over a railway bridge [51,52]. Before extracting the railway bridge response based on the on-board measured response, it was necessary to clarify the effect of bridge response on the track irregularity that was the input to each vehicle. However, most knowledge to date has been limited for bridge responses at the travel position with a moving single axis [14,49]. Most studies on these drive-by bridge inspection systems for railway bridges are based on numerical analysis; there are almost no actual field tests or full-scale experiments for drive-by bridge inspections in railways.

In this study, authors propose a drive-by system that detects resonant bridges [2,3,53] in high-speed railways, which are closely related to actual bridge states. The proposed filtering and enveloping process of track irregularities included the bridge displacement measured for the first and last vehicles; the process emphasized the vibration components unique to the resonant bridges, which were dominant only in the last vehicle. The resonant bridges could be detected using the difference between the processed track irregularities. The problem of frequency resolution [13], which was a bottleneck for drive-by systems of high-speed railways, was avoided by directly using the filtered and enveloped track irregularity waves measured for first and last vehicles. Furthermore, the effects of track irregularities excluding the bridge displacement components were considerably reduced by the difference between the measured data obtained from first and last vehicles. These novel and key ideas make it possible to realize a drive-by system for resonant bridges in high-speed railways, which has been difficult to date; these ideas provide certain insights for developing more sophisticated drive-by bridge inspection systems. Furthermore, the experimental validation of proposed methodology based not only on the on-board measured track irregularities but also on *in situ* measured bridge displacement responses in real high-speed railways can provide high reliability. Furthermore, the proposed method can directly use the in-vehicle track irregularity measurement system [45,54] and the track maintenance management database system [55,56] that are already extensively used for Japan's high-speed railways. Thus, the practical application of this study can be confirmed without making any additional investments.

The method proposed in this study has the following limitations. First, the theoretical and numerical calculations in this study assume constant train speeds. This is not a serious limitation because high-speed railways have long intervals between stations, and most trains run at a constant speed. Second, this study focuses only on the simply-supported bridges with the most basic structure, which are numerous in Japan's high-speed railways. Continuous bridges are outside the scope of this paper. Certain experimental results of its possible applicability to continuous bridges have been observed in the experimental validation, but theoretical verification is required for this in the future. The detection method proposed in this study can theoretically detect secondary resonance by adjusting the filtering passband. However, priority was given to the primary resonance, which causes various problems. Consequently, the secondary resonance was excluded from this study. Displacement at the mid-span of bridges under train passages is more common as a bridge performance index than the presence or absence of resonance [57–59]. This is not a direct limitation of drive-by resonance detection method proposed in this study; however, even if the proposed method is improved, the mid-span displacement response cannot be estimated using the principle of the proposed method. However, the key ideas and insights that can be used for the drive-by estimation of bridge displacement responses are provided in the numerical validations of this study.

2. Drive-by resonant bridge detection method

2.1. Resonance of railway bridges

To understand resonant bridges and drive-by detection method discussed in this study, the resonance phenomenon of railway bridges during train passages is explained. Authors discuss certain typical results of numerical simulation by considering the interaction between a railway bridge modeled as a 2D simply-supported beam and a train modeled using a 2D multibody vehicle. The details of the simulation model are given in Appendix A. For general high-speed railway bridges and vehicles in Japan, bridges and trains have the following specifications: a span length of 50 m, bridge fundamental frequency of 2.8 Hz, modal damping ratio of 2%, bridge unit length mass of 25 t/m, vehicle length of 25 m, bogie center interval of 17.5 m, bogie axle interval of 2.5 m, axle loads of 120 kN, and 12 vehicles per train. Other specifications were set as in [52].

Fig. 1 shows the bridge maximum response values and the displacement and the impact factor during train passage as a function of the train speed. Impact factors are commonly used in bridge designs [3,59]. The impact factor is obtained by subtracting 1 from the maximum bridge displacement divided by the static displacement. The maximum displacement and impact factor amplify rapidly at the train speed of ~ 250 km/h. Resonance occurs when the excitation frequency of the passing train represented by the vehicle length and train speed matches the bridge fundamental frequency. Fig. 2 shows the displacement time-series responses at the bridge mid-span with train speeds of 200, 230, 250, 270, and 300 km/h indicated by A, B, C, D, and E in Fig. 1. The horizontal axis represents the dimensionless time, where 1 is the time required for the passing of one 25-m vehicle. The displacement response at a train speed of 250 km/h (C) gradually increases with the passage of the train, and the maximum displacement occurs at the passage of the last vehicle. In B and D, a beat phenomenon occurs in which the bridge response amplitudes increase and decrease when the train passes over the bridge. The beat phenomenon occurs when two waves with slightly different frequencies overlap. In a high-speed railway bridge, these two frequencies are the excitation frequency of a traveling train and bridge frequency. Therefore, the beat phenomenon occurs when the train passes over a bridge at a speed that is slightly shifted (i.e., B and D) from the resonance speed.

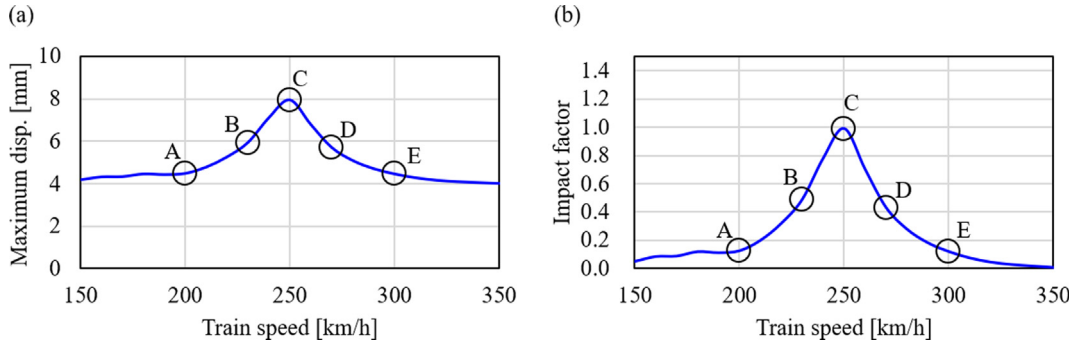

Fig. 1. Maximum response value of a simply-supported bridge during train passage as a function of the train speed: (a) Maximum displacements at the bridge mid-span and (b) Impact factors.

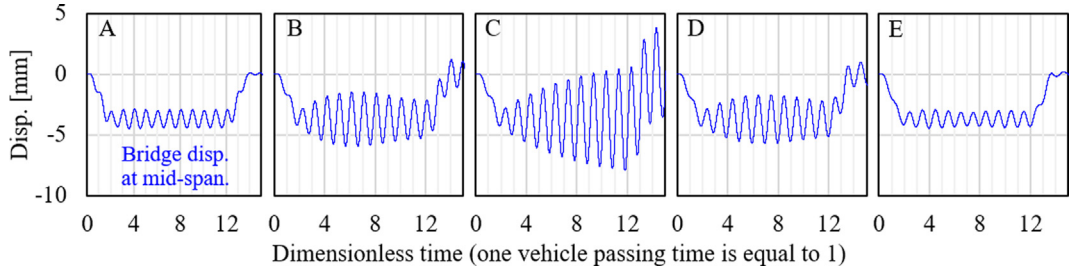

Fig. 2. Bridge mid-span displacement ("Disp." on the vertical axis) time history response for trains.

Resonance occurs when the excitation frequency corresponding to the regular axle spacing matches the bridge frequency. Therefore, the resonance train speed $v = v_{res}$ satisfies the following condition [53]:

$$v_{res} = f_0 \cdot L_a \tag{1}$$

where f_0 is the bridge fundamental frequency of the primary bending mode, and L_a is regular axle spacing. Regular axle spacing has several lengths such as the distance between the axles in a bogie or the distance between the centers of the bogies. However, the vehicle length L_c is the dominant excitation interval for medium and long-span bridges as shown in Fig. 1 and Fig. 2. Therefore, $L_a = L_c$ (25 m) is assumed in this study. Substituting the conditions shown in Fig. 1 into Eq. (1) and $L_a = L_c$ (25 m) gives $v_{res} = 2.8 \cdot 25 = 70$ m/s, which is ~250 km/h. The amplification of the bridge dynamic response by resonance is quite important in the design of high-speed railway bridges. Theoretical, experimental, and numerical studies have been conducted worldwide on interactions with vehicles, and these studies have been systematized as a design method using the impact factor [3,6,59,60].

2.2. Proposed method

In this study, authors propose a method for detecting resonant bridges based on track irregularities dynamically measured by devices placed on two vehicles of a running train. Using measuring devices mounted on the bogies of first and last vehicles, two track irregularities can be obtained. The track irregularity mentioned here includes the bridge displacement response.

In resonant bridges, the basic idea is to detect the difference in track irregularities estimated using different vehicles. Track irregularities measured at two points (i.e., at two locations of a train) include both static and dynamic bridge responses and rail irregularities. Assuming that rail irregularity does not change if measured at two different instants, its contribution to the signals acquired at the two points, which are then synchronized, is common. However, if the passage of the train modifies (and amplifies) the bridge dynamic response, since the measurements of the same point take place at different times, the estimations of rail irregularity using both sensors are different because of the movement of the bridge itself. Therefore, using a difference processing of the track irregularity measured at two train locations, the components amplified by the bridge dynamic response can be extracted.

A similar concept was proposed by Nagayama et al. [26] for road bridges where cross-spectrum analysis was used to extract the bridge vibration components common to two passing vehicles; however, it cannot be applied to high-speed railways because conversion to the frequency domain causes a significant lack of resolution. For this reason, we propose a new

method in the time domain that can extract resonant bridge responses directly using track irregularity data as a function of the position on the bridge.

This concept is briefly explained using the examples reported in Figs. 1 and 2. If resonance does not occur in the passing bridge as happen in A and E of Fig. 2, it is possible that the track irregularity measured on each bogie of the first and last vehicles will be almost the same. This is limited to the case in which the weight and length of the first and last vehicles are almost the same, a condition that is usually satisfied for high-speed rail vehicles in Japan since the capacities of the first and last vehicles are the same and limited to passengers (thus, the variation in weight is relatively small). Furthermore, even if resonance occurs in the bridge, as happen in C in Fig. 2, the track irregularity measured on the bogies of the first vehicle is almost the same as in the case of non-resonance. Nevertheless, track irregularity measured on the bogies of the last vehicle is also attributed to the overlap with the bridge response, which is amplified by resonance. Fig. 3 shows the bridge displacement at the center of the first and second bogies of the first and last vehicles when passing through the bridge (Fig. 2). As expected, in the resonance situation (C), the track irregularity measured by the last vehicle is significantly larger than that measured by the first vehicle.

2.3. Bogie-mounted track irregularity measuring device

The proposed method was validated using instrumentation already installed on the bogies of certain high-speed trains in Japan for measuring track irregularity [45,54]. Since this is a very common situation and ad-hoc sensors are not required, the proposed method can be implemented without specific investments; this is a particular advantage of this study. For equipment development and accuracy verification, please refer to [45,54]; this study provides only a brief description, focusing on the details useful for this research.

Fig. 4 shows the bogie-mounted track irregularity measurement device that is based on inertial measurements. The device comprised a gyroscope, an accelerometer, and four laser displacement meters. The gyroscope and the accelerometer estimate the position and attitude of the measuring device at each instant using second-order integration. The track irregularity is obtained subtracting the bogie displacement measured by the inertia measurement unit (IMU) from the relative displacement between the bogie and the rail measured through lasers.

For Japanese track maintenance, track irregularity is evaluated using the chord-based method. The mid-chord method evaluates the displacement distance from the rail to the average displacement of the front and rear points. In Japan, the 40-m mid-chord method is commonly used; this method measures the relative displacement with respect to average values at 20 m positions at the front and back of a target point as shown in Fig. 4 (c). The device was designed to cancel the influence of long wavelength components (i.e., low-frequency) applying the filter characteristic applied using the mid-chord method to the inertial measurement. The technical features of track irregularity measured by this device are the same of the general track-inspection trains, i.e., vertical, horizontal, and rotation irregularities. The accuracy has already been verified by field tests to be of the same quality as a dedicated inspection train [45]. Although it is difficult to restore long wavelength components, they can be ignored for the purposes of this study because their effect on the detection of resonant bridges is negligible.

Certain high-speed trains in service in Japan have devices installed on their first and last vehicles to prevent data loss in case of device failure and to compensate for decreased accuracy at low train speeds.

2.4. Resonant bridge's dominant vibration

In addition to bridge vibration, multiple vibration components are mixed in the track irregularity measured by the first and last vehicles. As described in Section 2.2, components other than the bridge displacement components were significantly canceled by the differential processing of track irregularities measured in first and last vehicles. However, if the vibration component unique to the resonant bridge is known, the highly accurate detection of the resonant bridge can be realized by signal processing that emphasizes the component. Here, a simple theoretical discussion on the resonant bridge displacement component measured just below the bogies (i.e., loading points) of first and last vehicles is explained.

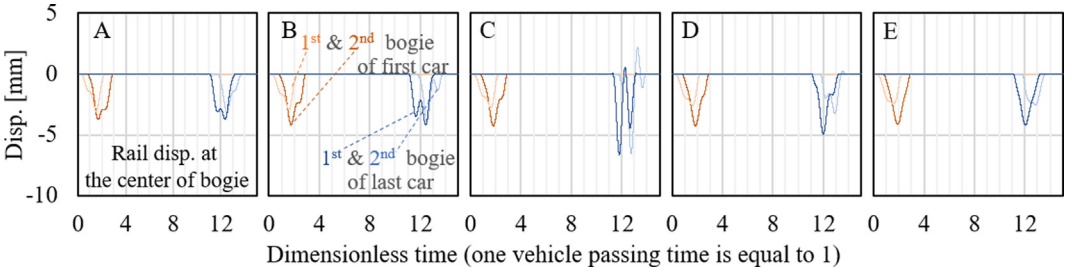

Fig. 3. Bridge displacement ("Disp." in the figure) responses at each train position and each train speed (i.e., bridge displacement component for the track irregularity).

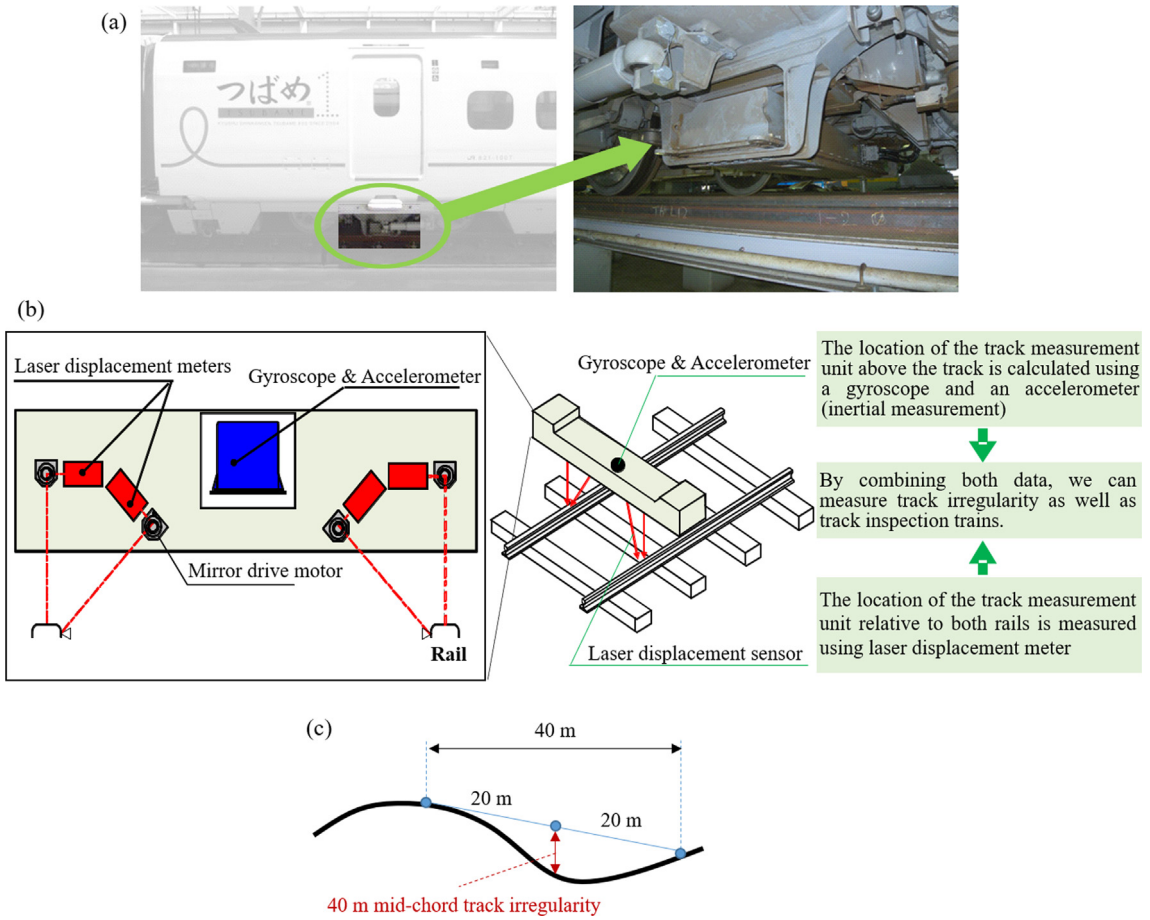

Fig. 4. Bogie-mounted track irregularity measurement device: (a) Measurement device actually introduced and (b) Measurement principle of track irregularity using inertial and displacement measurements.

Fig. 5 shows a theoretical model for analyzing the resonant bridge displacement component, which is measured as the track irregularity at the point of load application. The train load was idealized as a concentrated load sequence introduced at intervals along the vehicle length. Such idealization is often used for bridge resonance analysis [61]. Here, we focus on the bridge displacement at a certain point for the concentrated moving load. Here, it is assumed that the number of vehicles is considerably larger than that required to reach a steady state of bridge vibrations.

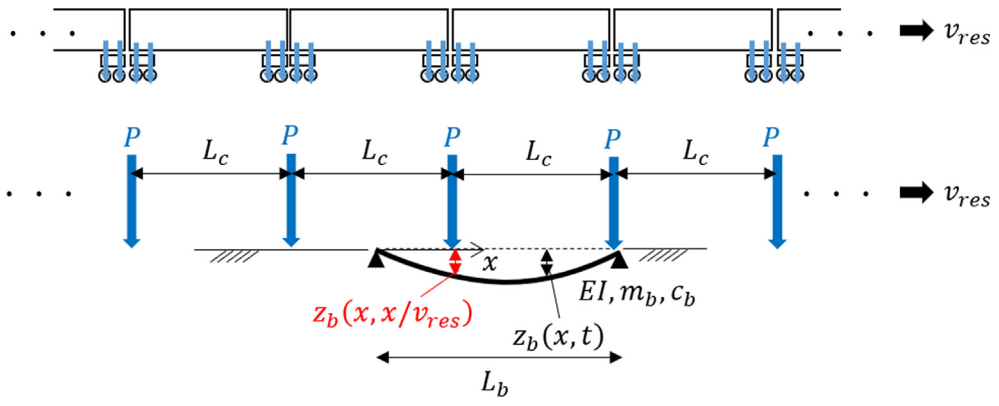

Fig. 5. Theoretical analysis model of resonant bridge response. L_c is the vehicle length; P is the concentrated moving loads for each vehicle length; v_{res} is the train speed (resonance speed); EI, m_b,c_b, and L_b are the bridge-bending stiffness, the unit length mass, the damping constant, and the span length; $z_b(x,t)$ represents the bridge's vertical displacement at the position x and the time t on the bridge.

The condition for resonance is given in Eq. (1). Therefore, the bridge frequency under the resonance condition naturally satisfies the following relationship:

$$f_1 = \frac{v_{res}}{L_c} = \frac{x}{L_c t} (0 \le x \le L_b) \tag{2}$$

where x represents the position in the longitudinal direction (the left end of the bridge is 0), t represents the time when the first concentrated moving load enters the bridge at the point 0, and L_b represents the bridge span length. The bridge displacement component at resonance comprises the following two components: the quasi-static deflection component $z_{b,s}(x,t)$ that depends on the position of the moving loads and the dynamic response component $z_{b,d}(x,t)$ that depends on the bridge frequency, modal damping ratio, and the magnitude of P [53].

$$z_b(x,t) = z_{b,s}(x,t) + z_{b,d}(x,t) \tag{3}$$

The quasi-static deflection component $z_{b,s}(x,t)$ does not change with the focusing vehicle because it depends only on the wheel load and wheel position. Assuming that the excitation frequency resonates with the primary bending mode of the bridge, the dynamic response $z_{b,d}(x,t)$ of the simple beam when passing through the train can be approximated as follows:

$$z_{b,d}(x,t) \approx \xi_{1,d}(t) \sin\left(\frac{\pi x}{L_b}\right) \tag{4}$$

Based on the steady-state assumption, the modal displacement $\xi_{1,d}(t)$ has the following relationship:

$$\xi_{1,d}(t) = A_{res} \sin(2\pi f_1 t + \theta_{res}) \tag{5}$$

where A_{res} represents the dynamic response amplitude at resonance. At resonance, the applied load and response amplitude are out of phase by $\pi/2$. Therefore, we have

$$\theta_{res} = \pi\left(1 - \frac{L_b}{L_c}\right) \tag{6}$$

2.5. Loading-point dynamic response of resonant bridges

Focusing on the dynamic displacement of the arbitrary mth loading point after the steady state, if the time t_m is defined as the time when the mth load enters the bridge, $z_{b,d}(x,t_m) = z_{b,d}(x, x/v_{res})$ can be obtained from the relationships $t_m = t - \{(m-1)L_c\}/v_{res}$ and $t_m v_{res} = x$ for $0 \le x \le L_b$. Using the relationship between Eqs. (4) and (5), the bridge dynamic displacement response at the mth loading point $z^m_{b,d}$ can be expressed as a function of only the position x as follows:

$$z^m_{b,d}(x) \approx A_{res} \sin\left(2\pi \frac{x}{L_c} + \theta_{res}\right) \sin\left(2\pi \frac{x}{2L_b}\right) (0 \le x \le L_b) \tag{7}$$

Fig. 6 shows an example of the bridge dynamic displacement component at resonance at the loading point obtained by Eq. (7) when the bridge span is 50 m and $A_{res} = 1$. Equation (7) shows that the maximum amplitude of the wave with the vehicle length L_c varies with $2L_b$, which is twice the bridge length. Therefore, the passed bridge can be judged as a resonant bridge if a vibration having the wavelength of the vehicle length can be observed and if the vibration amplitude is varied at the same period as the bridge length in the bridge displacement at the loading point, which is measured on the last vehicle passing over the bridge. However, the track irregularity measured at the loading point when passing through the bridge includes various components, such as rail corrugation, quasi-static bridge deflection and measurement noise, in addition to the resonance bridge response component given in Eq. (7).

2.6 Extraction of the resonant-bridge dynamic response component

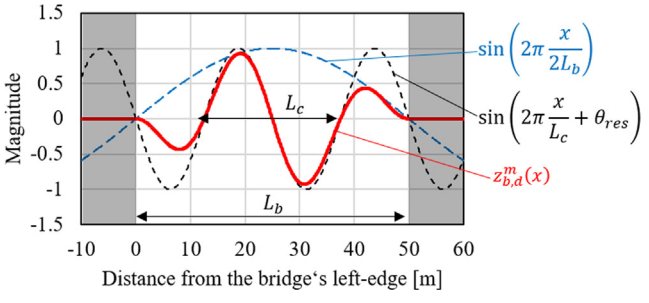

Fig. 6. Theoretically calculated bridge dynamic displacement components in resonance at the loading point for vehicle length of 25 m (bridge span = 50 m).

The track irregularities $l^f(x)$ and $l^l(x)$ of the loading points (including the bridge displacement components and measurement errors) measured by the first and last vehicles are given as follows:

$$l^f(x) = z^f_{b,s}(x) + z^f_{b,d}(x) + r(x) + e^f(x), l^l(x) = z^l_{b,s}(x) + z^l_{b,d}(x) + r(x) + e^l(x), (0 \le x \le L_b) \tag{8}$$

where$r(x)$ represents the track irregularity excluding the bridge displacement and measurement noise components; $r(x)$ can be modeled by normal distribution using the mean 0 and the variable variance σ^2, which usually decreases on the short wavelengthλ, as stated in [62]. $e^f(x)$ and $e^l(x)$ represent the measurement errors of bogie-mounted measurement devices on the first and last vehicles, respectively.

Here, as shown in Fig. 3, that the downward convex half sine wave observed during non-resonance (A and E) primarily corresponds to the quasi-static bridge displacement component $z_{b,s}(x)$ as shown in Eq. (3). Furthermore, the higher-frequency vibrations seen in the track irregularities recorded by the last vehicle at resonance C correspond to the dynamic displacement component $z_{b,d}(x)$ of the bridge. As noted in the track irregularities measured by the first vehicle in Fig. 3, the changes in the quasi-static bridge deflection component $z_{b,s}(x)$ in the first and last vehicles are sufficiently small, that is, $z^l_{b,s}(x) \approx z^f_{b,s}(x)$ because the $z_{b,s}(x)$ caused by the train load depends only on the wheel load and its loading position. However, as shown in Fig. 3, even in resonance state C, track irregularity measured by the first vehicle is primarily composed of a downwardly convex half sine wave, while the high-frequency dynamic displacement component measured by the last vehicle is not observed. Therefore, the relationship of $z^l_{b,d}(x) \gg z^f_{b,d}(x)$ is established for the bridge dynamic component $z_{b,d}(x)$ at resonance, such as situation C. Furthermore, the same measurement devices are used for track irregularity measurements; therefore, we can assume that the measurement errors $e^l(x)$ and $e^f(x)$ are generated from the same probability distribution. We assume a normal distribution$N(0, \sigma^2)$ with the mean 0 and variance σ^2 for distributing the measurement error. The additive nature of the variance $e^l(x) - e^f(x)$ can be expressed as the measurement error $e'(x)$ following the normal distribution $N(0, 2\sigma^2)$ with the mean 0 and the variance 2σ. Based on these discussion and Eq. (8), we can eliminate the track irregularity excluding the bridge displacement $r(x)$ and the quasi-static deflection component $Z_{bs}(x)$ by subtracting the $l^f(x)$ measured on the first vehicle from the $l^l(x)$ measured on the last vehicle:

$$l^l(x) - l^f(x) = z^l_{b,s}(x) + z^l_{b,d}(x) + e^l(x) - z^l_{b,s}(x) - z^l_{b,d}(x) - e^f(x) \approx z^l_{b,d}(x) + e'(x) \ \ (0 \le x \le L_b) \tag{9}$$

$$e'(x) \sim N(0, 2\sigma^2) \tag{10}$$

In Eq. (9), $z^l_{b,d}(x)$ is the product of sine waves with the vehicle length L_c and with twice the bridge length $2L_b$, as shown in Eq. (7) and Fig. 6. In real vehicles and resonant bridges in Japan's high-speed railways, the following relationship exists between L_c and $2L_b$. The length of a general high-speed railway vehicle L_c in Japan is 25 m; however, the span that may cause resonance in Japan's high-speed railway bridges is $\sim L_b \ge$30 m. See Appendix B for details on the relationship between the fundamental frequency and the span of high-speed railway bridges in Japan. Therefore, the relationship $1/L_c \gg 1/2L_b$ is given for the two wavelengths in Eq. (7) in most resonant bridges. As shown in Fig. 6, Eq. (10) is primarily composed of vibrations with wavelength L_c, and its amplitude varies at the wavelength $2L_b$. The domain is $0 \le x \le L_b$; therefore, the vibration component of the wavelength $2L_b$ does not have a large dominant component in the frequency domain. Figure 7 shows a typical example of a Fourier amplitude of the bridge dynamic displacement component $z^l_{b,d}(x)$ for the 50-m bridge span in Fig. 6. Only one peak with a vehicle length of 25 m could be confirmed.

For track irregularities measured in the real world, it is problematic to accurately extract $z^l_{b,d}(x)$ because of the effects of multiple errors. In addition to the simple measurement error $e'(x)$, the error factors include the position identification errors (for conversion from the observation time t to the position x). In position identification, errors occur depending on the changes in the distance between the first and last vehicles; these errors occur because of the degree of freedom of the rail direction and the distance of the communication terminals from the location identification devices installed on the ground. The difference between the waves with position identification errors result in an apparent wave, which does not actually exist. This becomes more prominent for the displacement responses with short wavelengths. Furthermore, there is a certain amount of the track irregularity component with the 25-m wavelength for the track irregularity measured on the first vehicle passing over a bridge that does not have any dynamic response because of bridge resonance. Therefore, to reduce unnecessary factors and to make the differential processing more robust against position identification errors, we performed two signal processing methods on the measured track irregularities using the characteristics of the measured bridge dynamic displacement component represented by $z^l_{b,d}(x)$. Figure 8 shows the workflow of the proposed detection method explained below.

One method was the bandpass filter processing that was used to remove vibrations other than the main component of the vehicle length shown in Figure 7 from the measured track irregularities of the device shown in Fig. 3. In this study, we called the filtered irregularities as the vehicle length irregularity. Another method is envelope processing in which the vehicle length irregularity amplitude was estimated by enveloping. If $F\{\cdot\}$ is the bandpass filtering, and $G\{\cdot\}$ is the enveloping, the track irregularities that include the bridge displacement of the first and last vehicles after each processing can be expressed by the following two equations:

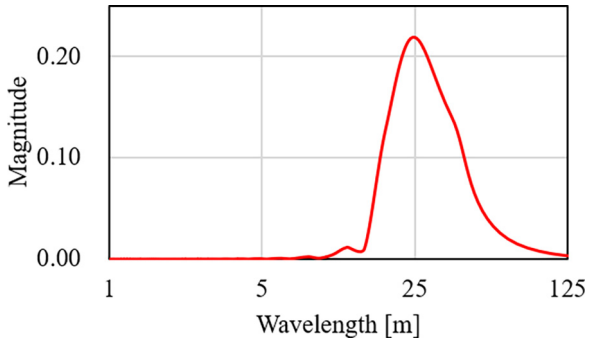

Fig. 7. Fourier amplitude of bridge dynamic displacement component at resonance at the loading point for a vehicle length of 25 m (bridge span = 50 m).

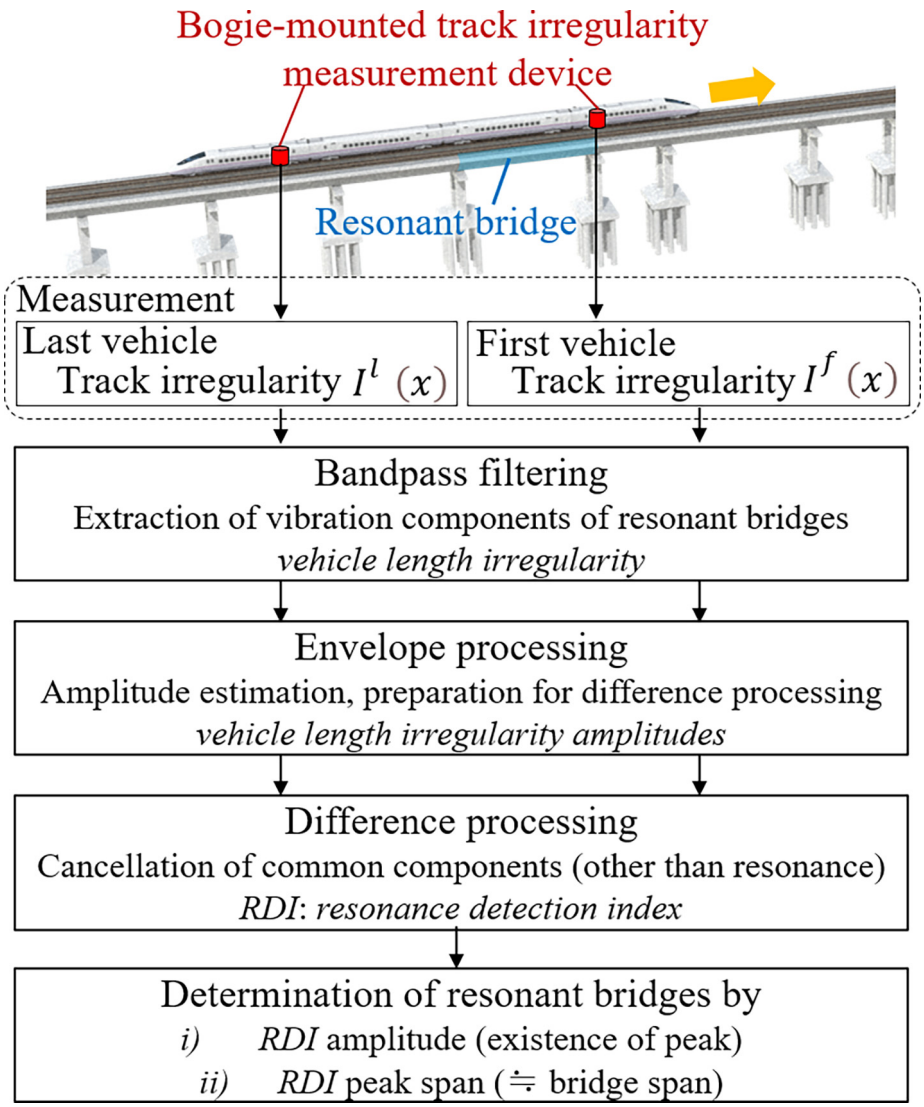

Fig. 8. workflow of the proposed detection method.

$$G\left\{F\left\{I^f(x)\right\}\right\} = G\left\{F\left\{z^f_{b,s}(x)\right\} + F\left\{z^f_{b,d}(x)\right\} + F\{r(x)\} + F\{e^f(x)\}\right\} \approx G\left\{F\left\{z^f_{b,s}(x)\right\}\right\} + \sigma_{Ir,L_c} + \sigma_{e,L_c} \tag{11}$$

$$\begin{aligned} G\left\{F\left\{I^l(x)\right\}\right\} &= G\left\{F\left\{z^l_{b,s}(x)\right\} + F\left\{z^l_{b,d}(x)\right\} + F\{r(x)\} + F\{e^l(x)\}\right\} \\ &\approx A_{res,F}\sin\left(2\pi\frac{x}{2L_b}\right) + G\left\{F\left\{z^l_{b,s}(x)\right\}\right\} + \sigma_{Ir,L_c} + \sigma_{e,L_c} \end{aligned} \tag{12}$$

where σ_{Ir,L_c} and σ_{e,L_c} represent the amplitudes of the measurement error and the filtered irregularity without the bridge response components. $A_{res,F}$ is the amplitude of the resonant bridge dynamic displacement component after bandpass filtering. The difference in the track irregularities measured on the first and last vehicles after this processing can be approximated by the following equation:

$$G\left\{F\left\{I^l(x)\right\}\right\} - G\left\{F\left\{I^f(x)\right\}\right\} \approx A_{res,F}\sin\left(2\pi\frac{x}{2L_b}\right).(0 \le x \le L_b) \tag{13}$$

Enveloping involves estimating the blue dotted line from the red line in Fig. 6. Therefore, the component $z^l_{b,d}(x)$ observed only in the resonant bridge after enveloping is a convex function with the bridge span length being half a wavelength. Furthermore, a measurement error occurs when the differences between waves are increased because of the additive nature of variance. However, the measurement error component can be canceled by differential processing, which converts the error component into the amplitude of the measurement error by enveloping. In particular, the variance of the measurement errors for the first and last vehicles is considered to be comparable in principle because the same measurement devices were used for the first and last vehicles. Therefore, by enveloping, we can expect a high removal effect of the measurement error components. Moreover, by calculating the difference between the vehicular length irregularity amplitudes of the first and last vehicles after processing, we detected the resonant bridge as a half-wave convex peak corresponding to the bridge length. The convex wavelength of the resonant bridge estimated by the envelope processing is $2L_b$, which is at least twice the wavelength L_c. Therefore, even with the same position identification error, the error after difference processing can be suppressed to a value less than the difference processing of the wave with the wavelength L_c.

Based on the above data, we formulated the resonance detection index (RDI) as follows:

$$RDI(x) = G\left\{F\left\{I^l(x)\right\}\right\} - G\left\{F\left\{I^f(x)\right\}\right\}(0 \le x \le L_b) \tag{14}$$

Therefore, the following equation will determine whether the bridge with the span L_b over which the train has passed is resonating:

$$RDI(x) \propto \begin{cases} \sin\left(\pi\frac{x}{L_b}\right) & : Resonance \\ 0 & : Non\ resonance \end{cases} (0 \leqslant x \leqslant L_b) \tag{15}$$

The principle of this method is based on an idealized model. In the real world, RDI can have more complicated properties due to other effects such as axle arrangement, bogie positions for measuring track irregularities, the presence of the front and rear bogies, and the differences in the bridge quasi-static responses when the first and last vehicles pass over the bridge. In this study, we confirm the effects of various factors by numerical analysis and show their application to actual bridges and vehicles.

3. Validation results of the numerical model

3.1. Creation of simulated measurement track irregularities including bridge displacement components

In this study, we examined the effect of various factors on the detection accuracy of a resonant bridge using a numerical analysis result that considered the dynamic interaction between the vehicle and bridge for a simple support bridge. For calculating the bridge displacement component, we used a general 2D vehicle–bridge interaction simulation model [52,63–65]. The wheels and rails were rigidly connected, and track irregularities were considered as forced displacements. See Appendix A for details of the simulation model. The train was modeled by connecting 12 vehicles, as shown in Fig. 9. We used the specifications for a general high-speed railway vehicle used in Japan. The vehicle length L_c is 25 m and the bogie center interval is 17.5 m; the axle interval in a bogie is 2.5 m and the axle weight is 120 kN. Other specifications are the same as those in [52].

The bridge is assumed to be a standard simple-supported bridge in Japan's high-speed railway. The bridge span varies from 20 to 60 m, and the unit length mass is 25 t. The natural frequency is 2.8 Hz with a resonance speed of ~ 250 km/h. The modal damping ratio of bridges is set to 2% excluding Section 3.4. As shown in Appendix B, the lower limit of the bridge fundamental frequency of Japan's high-speed railway bridges generally corresponds to $55L_b^{-0.8}$. Therefore, concrete bridges having a 40 to 45 m span have a frequency of ~ 2.8 Hz in the real world. Although the fundamental frequencies of other span bridges are different from those of actual bridges, the bridge frequencies were set to 2.8 Hz (regardless of the span) to eliminate the influence of the resonance speed. To make the ratio of bridge displacements and various errors and irregularities almost the same as in reality, we adjusted the wheel loads such that the maximum deflection of the bridge at resonance was

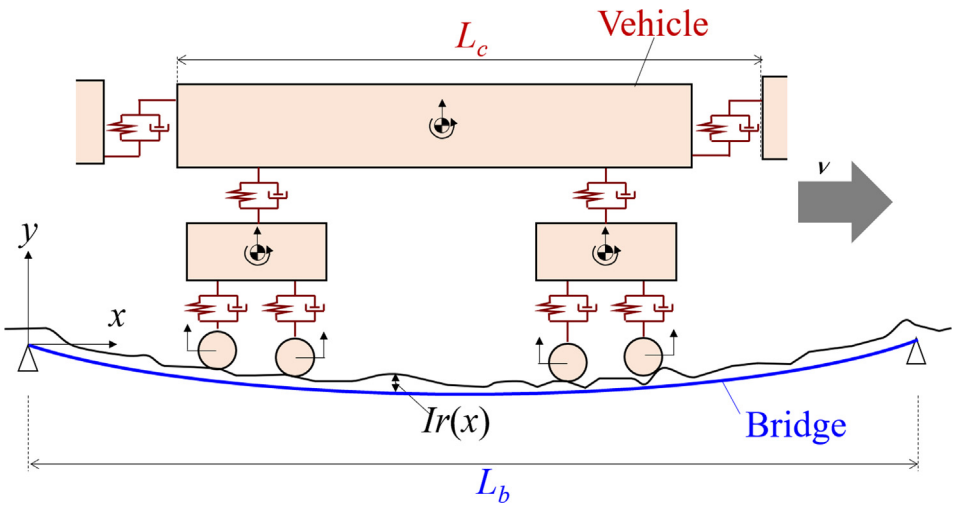

Fig. 9. Passage of a vehicle model with six degrees of freedom on a simple-supported beam

$L_b/2000$ mm. $L_b/2000$ mm was roughly equivalent to the upper limit of the measured vertical displacement in existing high-speed railway bridges in Japan [65].

The measurement error is generated by random numbers using a normal distribution. Based on the previous test results (which included inertial measurements) of the bogie-mounted track irregularity measuring devices, we reported the standard deviation of the measurement error at the 5-m mid-chord versine displacement (i.e., the relative displacement with respect to the average values at 20-m positions front and back of a target point) to be less than ~ 0.2 mm. Therefore, the standard deviation of the normal distribution that generates the random numbers is based on 0.2 mm.

Rail irregularities were characterized by Wiriyachai et al. [62] as one-sided power spectral density functions $S_{rr}(\Omega)$, where $\Omega = 2\pi/L_r$ rad/m is the spatial frequency or the wave number. L_r is the wavelength of the rail irregularity. In this study, we used the following equation proposed by Zhang et al. [66] and Lei and Noda [67] based on Wiriyachai et al. [62]:

$$S_{rr}(\Omega) = kA\frac{\Omega_c^2}{\left(\Omega^2 + \Omega_c^2\right)\Omega} \tag{17}$$

where k = 0.25 andΩ_c = 0.8245 rad/m. The value of the coefficient A is presented in Table 1.

The previously measured results on Japanese high-speed railways demonstrated that the maximum amplitude of rail irregularities was within ± 7 mm. In recent years, the measured value of a 5-m mid-chord versine displacement has a maximum of ~ 5 mm [68,69]. These values correspond to Grade 6 when compared with the values in Eq. (17) and Table 1 [66]. In this study, we consider Grade 6 based on these measurements of orbital irregularities.

The train speeds are to 200, 230, 250, 270, and 300 km/h corresponding to points A, B, C, D, and E of Fig. 1 respectively. These train speeds correspond to ± 10% and ± 25% of the resonance speed of 250 km/h. When converting the time-series response to distance, we perform resampling at 250-mm intervals in accordance with actual track irregularity measurements.

3.2. Effect of train speed

To confirm the basic performance of the proposed RDI, we applied the proposed method by assuming that the bridge displacement component is observed as track irregularity. Fig. 10 shows the results considering only the bridge displacement

Table 1
Coefficient A of rail irregularity power spectrum density.

Grade	Coefficient$A$
1	121.07
2	101.81
3	68.16
4	53.76
5	20.95
6	3.39

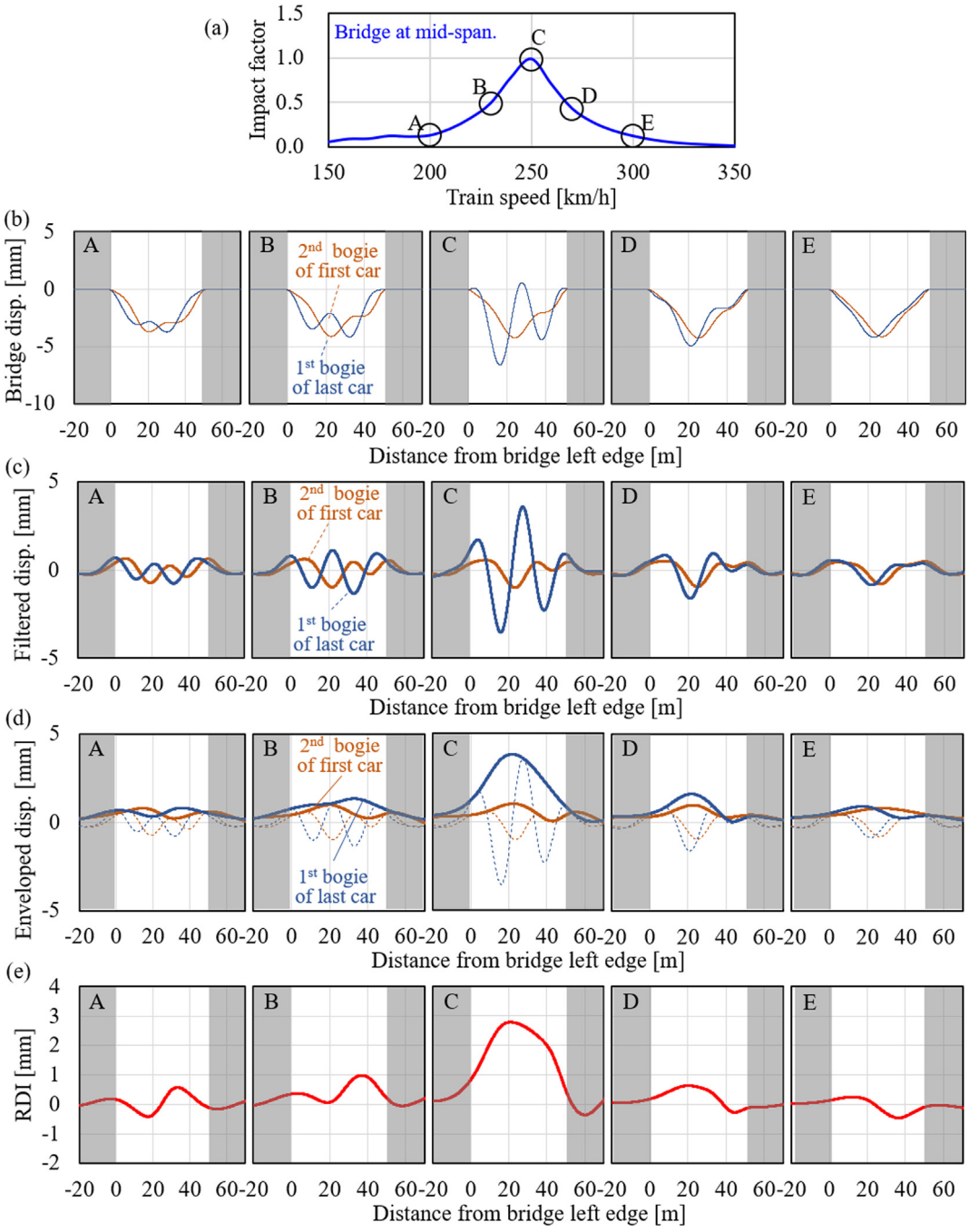

Fig. 10. Applied results only for the bridge displacement components (50-m span length): (a) Maximum displacements at the bridge mid-span as a function of train speed (same as Fig. 1); (b) Input track irregularities with only bridge displacement component; (c) Filtered vehicle length irregularities; (d) Enveloped vehicle length irregularities; and (e) Resonance bridge detection index.

components measured on the first and last vehicles. Fig. 10 (b) and (c) show the track irregularities (consisting only of the bridge displacement component) and the filtered vehicle length irregularities, respectively. Fig. 10 (d) and (e) show the enveloped vehicle length irregularity amplitudes and the RDIs calculated using the results in Fig. 10 (d), respectively. Fig. 10 (a) shows the same results as Fig. 1 for the resonance states A, B, C, D, and E for each of the speeds.

By comparing the vehicle length irregularities in Fig. 10 (c) with the input irregularities in Fig. 10 (b), we could eliminate only the quasi-static bridge displacement component with a long wavelength. However, even in the non-resonant states A and E, there are variations in the bridge displacement components because of the entry and exit of the bogies before and

after the bogies installed the measurement devices. The vehicle length irregularity amplitudes in Fig. 10 (d) are affected by these variations. There are slight differences between the first and last vehicles even in cases where there is no resonance.

As shown in Fig. 10 (d) and (e), the vehicle length irregularity amplitude of the last vehicle was much larger than that of the first vehicle in the resonance state C. Consequently, RDI forms a convex dominant component in the resonant bridge position. In the beating states B and D where the impact factors are approximately half that of the resonance, the RDIs rapidly attenuated to less than ~ 25% of the resonance. Furthermore, for non-resonant train speeds A and E, the RDI values are maximum at 15% of the resonance.

3.3. Effect of bridge span

Fig. 11 shows the RDI values when the bridge span is changed from 20 to 60 m. Track irregularity is introduced considering only the static and dynamic response components of the bridge. Fig. 11 shows that, in any span, RDI generates a convex-shaped outstanding component only at the resonance speed. Therefore, it is highly possible that the proposed method can be applied to a wide range of resonant bridges with span lengths ranging from 20 to 60 m. However, the maximum RDI value at resonance varies depending on the bridge span. The bridge span of 40 m is close to 1.5 times the vehicle

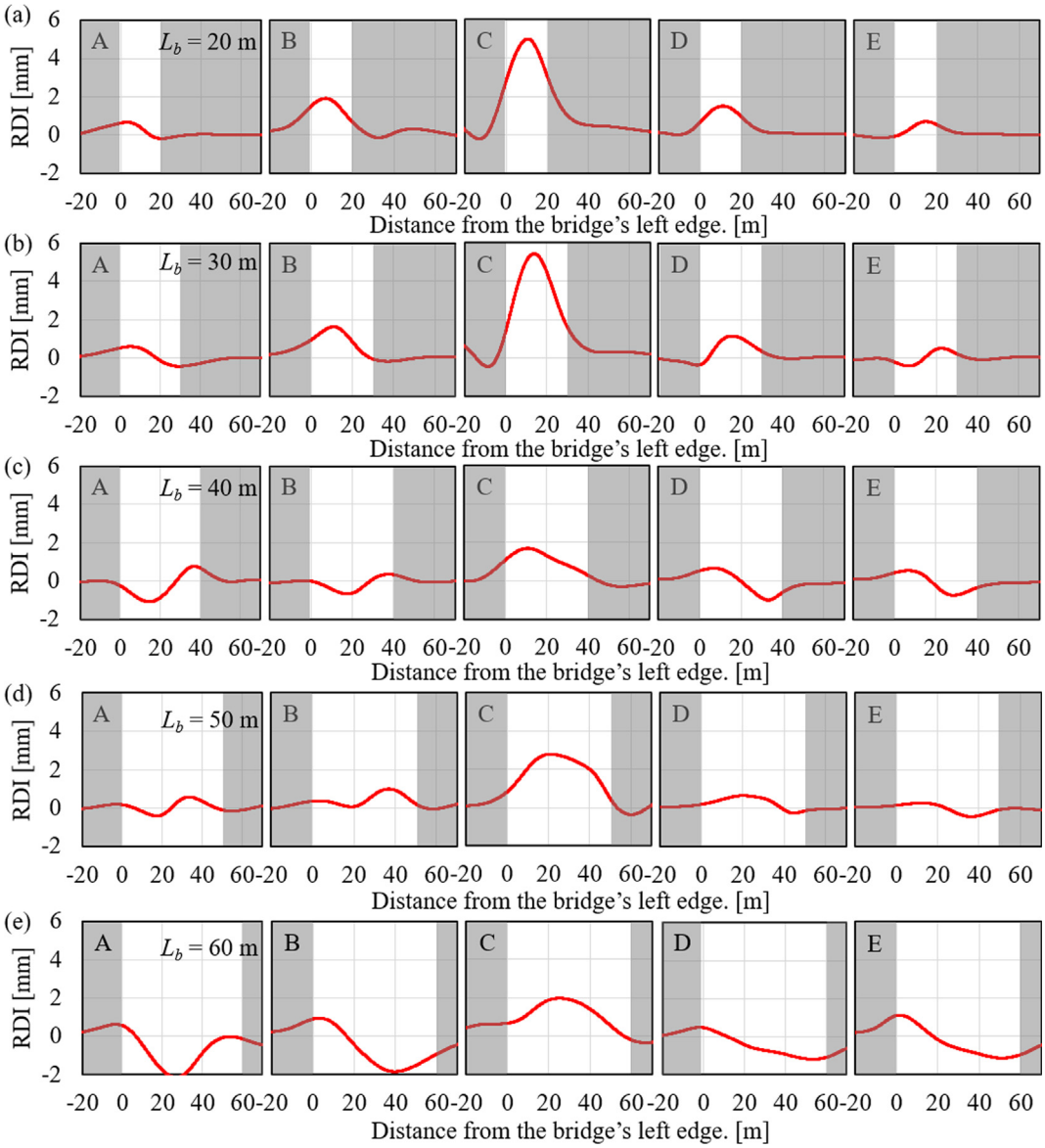

Fig.11. Applied results only for the bridge displacement components (train speeds correspond to speeds in Fig. 9 (a)): Bridge spans of (a) 20 m, (b) 30 m, (C) 40 m, (d) 50 m, and (e) 60 m.

length of 25 m (the bridge span that causes anti-resonance); therefore, the dynamic response component of the bridge is difficult to amplify even when there is resonance. Thus, the RDI at resonance was small as compared with other spans. Other bridge span effects were related to the number of vehicles on the bridge. The number of vehicles on the bridge increased as the bridge span increased. Then, the long-period bridge displacement component for the entire train is relatively larger. Therefore, with increase in bridge span, there is a reduction in the maximum RDI values at resonance.

By focusing on A, B, D, and E, which are not in the resonance state, we confirmed the tendency of RDIs to fluctuate to the negative side for bridge spans greater than 40 m. This is the effect of the quasi-static bridge displacement component that corresponds to the increase in the number of vehicles on the bridge. There is a large difference between the number of vehicles in the front and the rear of the first and last vehicles of interest in this study. For example, there are no vehicles on the bridge immediately after the first vehicle entered; however, there are many vehicles on the bridge after the first vehicle passed the long bridge mid-span. The situation is the opposite for the last vehicle. Therefore, the bridge quasi-static displacement components when passing the first vehicle tends to increase in the second half; however, the displacement components for the last vehicle tends to increase in the first half. This difference generates negative RDI fluctuations in the non-resonant situation. For bridge spans of 30 and 20 m, which are equal to or less than the vehicle length, we cannot confirm any RDI fluctuations on the negative side in the non-resonant states. Moreover, this fact supports the above considerations.

The RDI fluctuations at non-resonance correspond to the difference in the quasi-static bridge displacement components of the first and last vehicles because of the difference in the number of vehicles (measured by the number of wheel axles) on the bridge. Based on this, we can estimate the bridge displacement using RDI at non-resonance. This could be a future task; however, it is a feature worth mentioning for developing of a more general drive-by bridge inspection. The variation of maximum RDI values at resonance and the RDI fluctuation at non-resonance depend on the bridge span. However, we confirm that the resonance of high-speed railway bridges with general deflections ranging from 20 to 60 m can be detected in the ideal situation.

3.4. Effect of bridge damping

Fig. 12 shows maximum displacements at bridge mid-span with the bridge modal damping of 1%, 2%, and 5%. The effect of bridge damping on detection accuracy is verified by applying the proposed method to track irregularities when passing through these bridges with various bridge damping. The value of 2% is used as the bridge modal damping in Japanese bridge design code. However, a large variation in the measured bridge modal damping is present. In particular, investigating the case with large modal damping from the viewpoint of detection accuracy is necessary. Here, 5% is used as the case where the bridge modal damping is large in the concrete bridge. Furthermore, European design standards stipulate that the modal damping of steel and composite bridges is 1% for middle and long span. Therefore, 1% was also examined as an example of remarkable resonance.

Fig. 13 shows the RDI calculated from the track irregularities with 1%, 2%, and 5% of bridge modal damping. The effect of bridge damping has almost no effect on the RDI at non-resonance indicated by A and D in Fig. 13. Moreover, the RDI in resonance state C has the smallest amplitude when the modal damping is 5%. However, the fluctuation range of RDI is ~ 1 mm. Furthermore, predominant span of RDI is largely unaffected. From these results, it can be inferred that bridges with modal damping of<5% can be detected by the proposed method.

3.5. Effect of measurement error

In this section, the results of simulations considering the measurement error are shown. The error is introduced, generating a random number using the normal distribution with the three standard deviations of 0.1, 0.2, and 0.5 mm.

Fig. 14 shows examples of the simulated track irregularities for analyzing the effect of the measurement error for a bridge span of 50 m; the train speed is 250 km/h. The measurement errors of the first and last vehicles were separately generated from the same normal distribution, and these errors were added to the bridge displacement components of the first and last

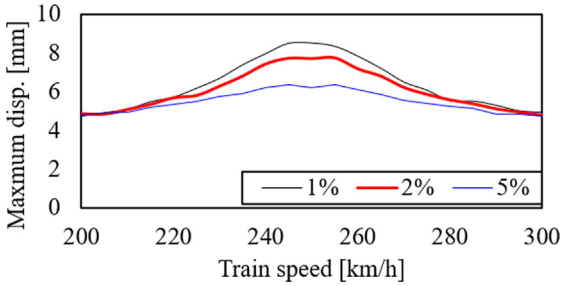

Fig. 12. Maximum displacement at the bridge mid-span with bridge modal damping 1%, 2%, and 5% (50-m span length). "Disp." Stands for the displacement.

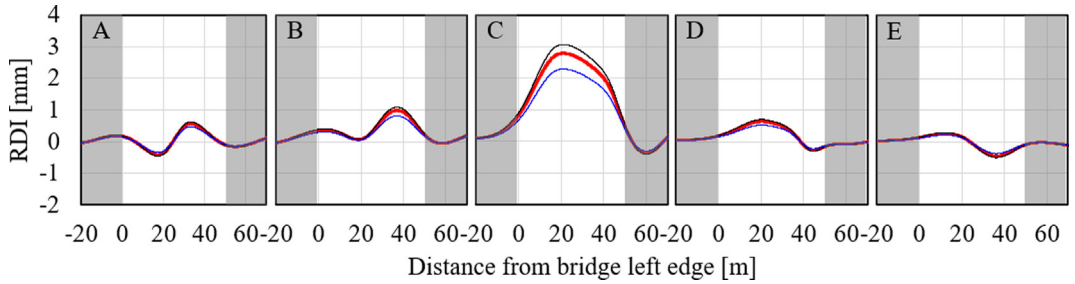

Fig. 13. Effect of bridge damping for resonant bridge detection (span = 50 m); the train speed corresponds to the speed in Fig. 9 (a)).

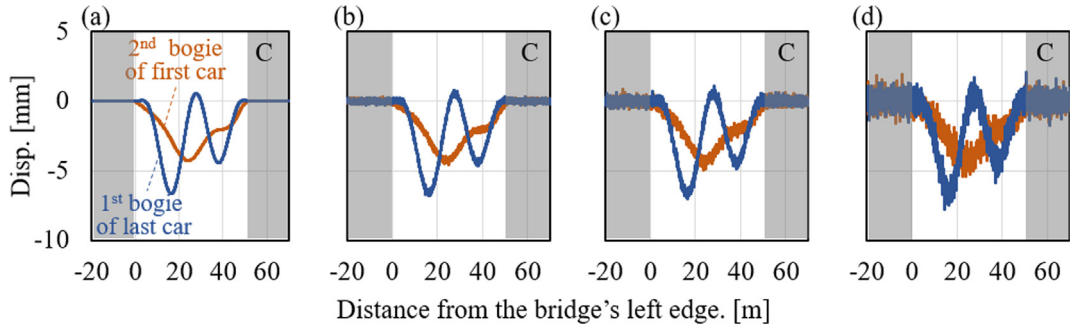

Fig. 14. Examples of simulated track irregularities with the bridge displacement component and measurement error (bridge span 50 m, train speed 250 km/h). Measurement error distribution with standard deviations of (a) 0 mm, (b) 0.1 mm, (c) 0.2 mm, and (d) 0.5 mm.

vehicles, respectively; the obtained results are shown in Fig. 15. The RDIs hardly change, even when the measurement error is 0.5 mm, which is more than double the practical measurement error. This tendency is the same in the other spans. Therefore, we can confirm that the resonance bridge can be detected by the proposed method regardless of the measurement error in the inertial measurement device being currently used.

3.6. Effect of track irregularities other than the bridge displacement components

The track irregularities are random; therefore, ten track irregularities were generated using Eq. (17) with Grade 6. By adding these irregularities to the bridge displacement component and measurement error (standard deviation = 0.2 mm), 10 simulated track irregularities were created. The same track irregularities were introduced in the first and last vehicles.

Fig. 16 shows examples of simulated track irregularities created for a bridge span of 50 m and a train speed of 250 km/h. By adding the track irregularity generated by Eq. (17), the simulated track irregularities greatly fluctuate.

Fig. 17 shows the results applied to the simulated track irregularities (bridge span = 50 m). RDI fluctuates in the range of approximately ± 0.5–±2 mm because of track irregularities. The maximum RDI value at the resonance state (C) tends to

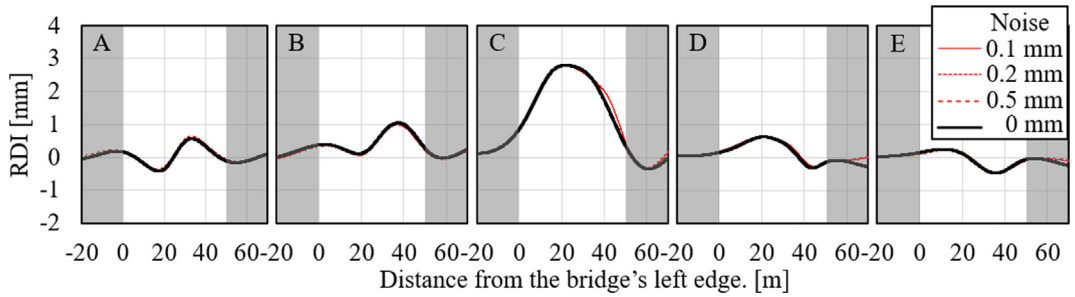

Fig. 15. Effect of measurement error on resonant bridge detection (span = 50 m; train speed corresponds to speed given in Fig. 9 (a)).

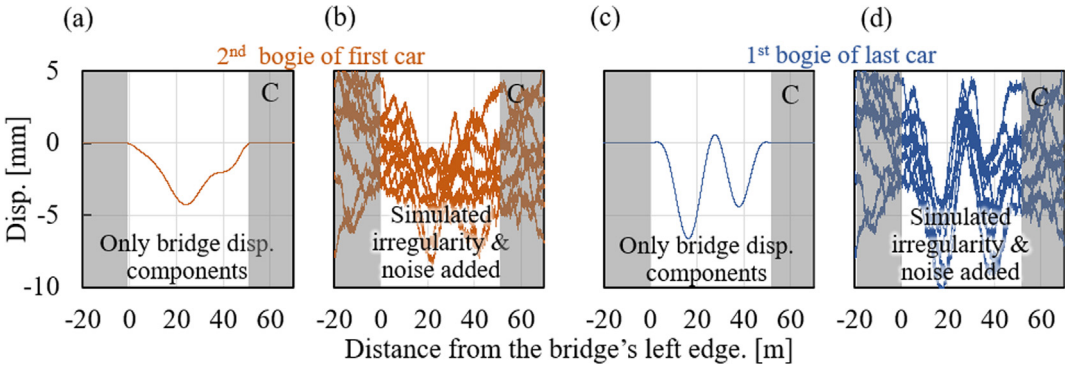

Fig. 16. Examples of simulated track irregularities with the bridge displacement component and measurement error (bridge span 50 m, train speed 250 km/h). Measurement error distribution with standard deviations of (a) 0 mm, (b) 0.1 mm, (c) 0.2 mm, and (d) 0.5 mm.

increase in the range of + 1 mm by the introduction of track irregularities. Although the dominant shape slightly changed by the addition of track irregularities in some cases, the dominant RDI components at resonance had a positive convex excellence with the half-wavelength of the bridge. The RDI fluctuation arising from the introduction of orbital irregularity is large when driving at a speed lower than the resonance speed. As shown in Fig. 10 (c), when the train passing speed is less than the resonance speed, the first and last vehicles show waves with different phases in the vehicle length irregularities with only the bridge displacement components. When track irregularity with the same wavelength as the vehicle length is overlapped to the bridge displacement component at a position with a large amplitude in the first vehicle, the vehicle length track irregularity of the first vehicle is amplified. However, the vehicle length irregularity of the last vehicle is canceled. Consequently, RDI, which is the difference between the irregularities, greatly changed. This fluctuation observed in RDIs is the largest at ± 2 mm when the resonance speed indicated by B is − 10%. For other train speeds, the RDI fluctuation is approximately ± 0.5 mm. The maximum RDI value at resonance is ~ 3 mm for a bridge span of 50 m. The RDI excellence at resonance with a span of 50 m is larger than the effect of fluctuations in track irregularities. Therefore, we could conclude that the existence of resonance can be judged by RDI even by considering the track irregularity effect. However, we need to be careful when comparing different bridges having the same spans but different track irregularities. There is a possibility that the state B before the resonance may be estimated as a resonance when the variation by track irregularity is quite different in the bridge to be compared. Even in this case, it is possible to improve the resonance bridge detection by referring to the on-board measurement results with different traveling speeds. Furthermore, this misdetection does not miss the resonant bridges. Therefore, we can confirm that the proposed method can detect the resonant bridges on the safe side using on-board measured track irregularities including the bridge displacement components, even in the presence of track irregularity and measurement noise.

Each bridge span (20–60 m) was examined considering the same track irregularity, and the RDI fluctuations had the same tendency. As typical examples, the results for bridge spans of 30 and 60 m are shown in Fig. 18. As shown in Fig. 18, the RDI values of bridges with 30 m are far superior to the RDI values of long-span bridges. Therefore, the resonant bridge can be easily detected even if the fluctuation of ~ 2 mm occurs by the added track irregularity. However, as shown in Fig. 18 (b), the effect of the track irregularity at the 60-m span is almost the same as that at the 50-m span. Nevertheless, the maximum RDI value for bridges with the span of 60 m at resonance is less than that for bridges having the span of 50 m; therefore, it

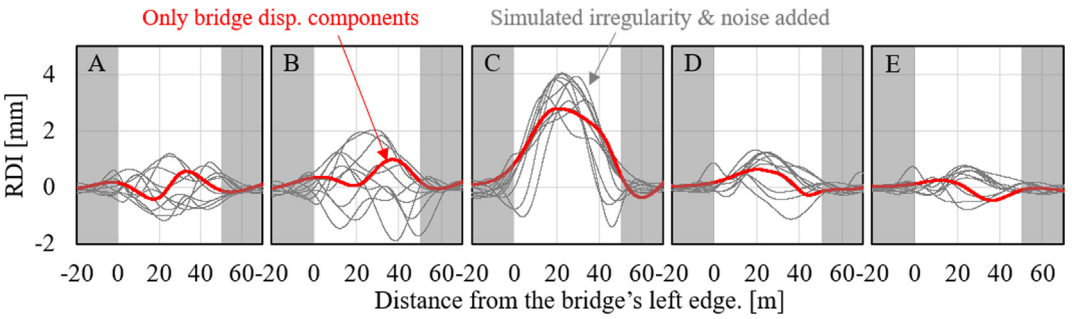

Fig. 17. Effect of track irregularities for resonant bridge detection (span = 50 m); the train speed corresponds to the speed in Fig. 9 (a)). "Disp." Stands for the displacement.

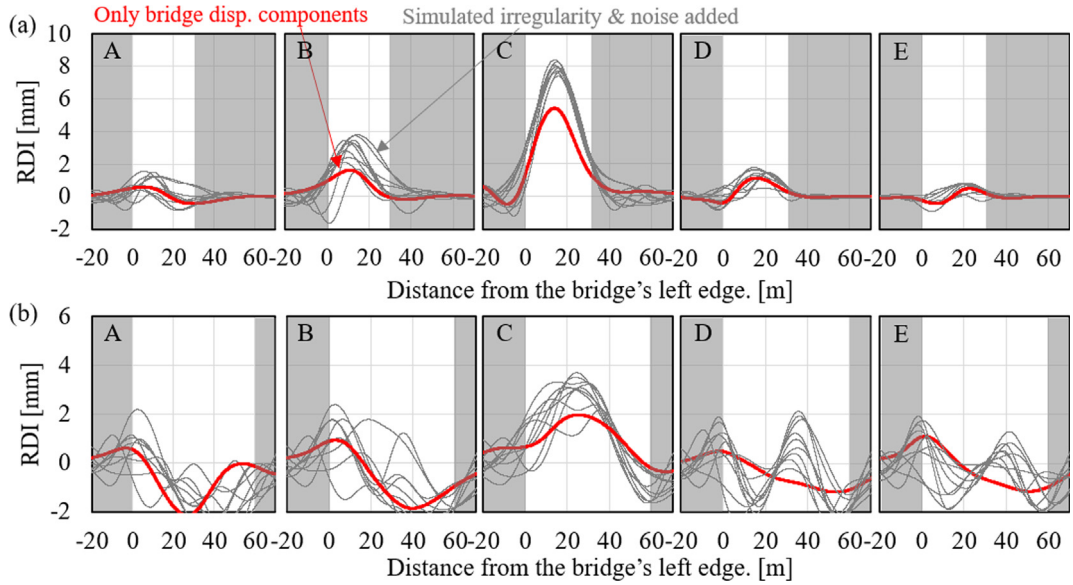

Fig. 18. Effect of track irregularities on resonant bridge detection (train speed corresponds to the speed given in Fig. 9 (a)). The bridge spans are (a) 30 m and (b) 60 m.

might be difficult to estimate the resonance state C and the beat state B separately as it was done for bridges having the span of 50 m.

In summary, except for the bridge span of 40 m, which has a small resonance amplification because of the anti-resonance bridge span, there is a high possibility that the bridge in the resonance state can be detected by the proposed method using a wide range of bridge spans ranging from 20 to 60 m.

3.7. Effect of position identification error

Track irregularity is recorded as a function of the time domain together with the train speed time-series. Then, for position identification, these values are converted into a distance function based on the communication records with the ground communication terminal. For high-speed trains in Japan, the communication records with the ground communication terminals for position identification are measured for both first and last vehicles. In this study, we used this information to estimate the positions of the second and first bogies of the first and last vehicles. Furthermore, to correct a small position identification error, position identification was repeated using the cross-correlation of the data of the last vehicle based on the measured data of the first vehicle [70]. Therefore, the position identification of the measured data for applying this study shown subsequently is usually < 1 sample (250 mm). However, a position identification error of ~ 1 m is generally unavoidable without enough ground communication terminals and precise position identification by cross-correlation. To confirm the accuracy of the proposed method in such a general measurement situation, we shifted the position of the last vehicle and applied the proposed method with a position identification error. Then, we calculated the RDI. We examined the situation when the last vehicle has position identification errors of 0 mm (none), ±250, ±500, ±1000, and ± 2000 mm with respect to the first vehicle.

Fig. 19 shows the effect of the position identification error on RDI when the bridge span is 50 m. Here, as described in 3.1, Grade 6, which is the closest to the actual situation of Japanese high-speed railways, was used. If the position identification error of the last vehicle relative to the first vehicle is in the range of ± 2000 mm, the influence of the position identification error on the RDI will be negligible. This is the case even when track irregularities are added. Note that if the bandpass filtered waveform is directly subtracted without the enveloping process, an error of up to ± 1.5 mm occurs even when the bridge span is 50 m. These results confirm that the proposed method is robust in the case of position identification errors between the first and last vehicles if the data are enveloped to increase the RDI wavelength.

Based on these confirmation results, bridges with RDI peak amplitudes greater than 1.5 mm and RDI peak spans matching the bridge span length were extracted as resonance. This simple threshold setting includes empirical findings obtained through trial and error based on next field test data. Consequently, more generalized thresholds that can be applied to fields other than those targeted in this study need to be set in detail according to span length and track irregularity management levels. This issue should form the basis of future work.

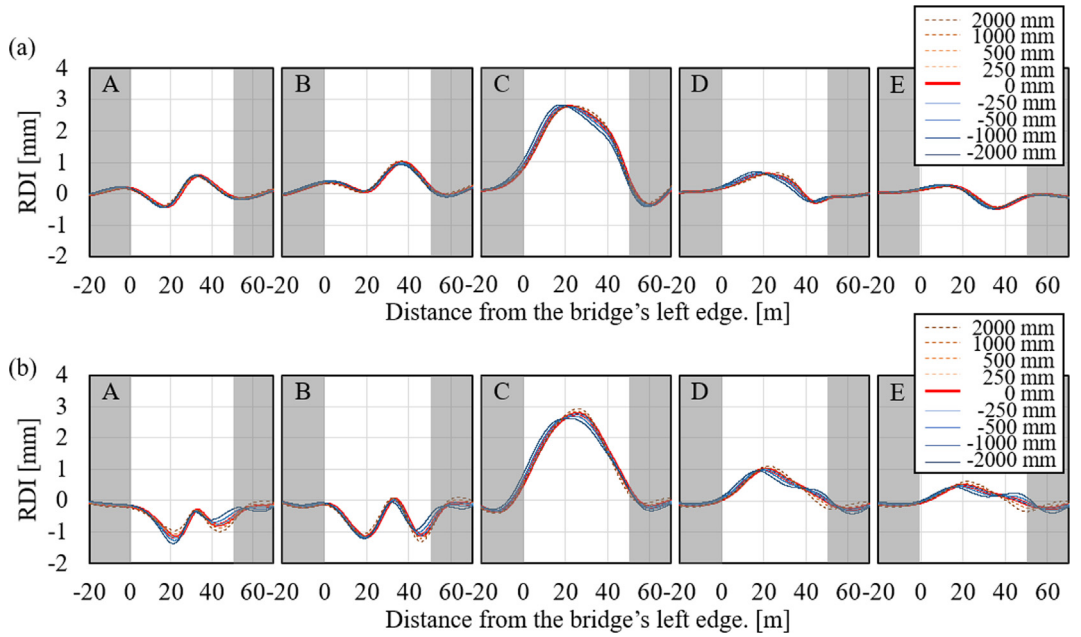

Fig. 19. Effect of the position identification error on the resonance bridge detection with (a) only the bridge displacement component and (b) the bridge displacement component and track irregularity. The bridge span was 50 m, and the train speed corresponded to the speed given in Fig. 9 (a).

4. Validation results on actual high-speed railways

4.1. On-board measurement method

For our application, we selected one of Japan's high-speed railway lines on which certain service trains are running with their first and last vehicles fitted with track irregularity measuring devices. Of the total length of ~ 250 km, the target stretch is ~ 22.6 km (875 bridges) excluding the acceleration/deceleration sections before and after the stations, the sections on embankment and the tunnels. The selected train was composed by eight vehicles. The geometrical characteristics of these vehicles are the same as those used and have an axle weight of ~ 110 kN without passengers. The travel speed in the target section was ~ 230–250 km/h. The track irregularity measuring devices were installed in the center of the second and first bogies of the first and last vehicles, respectively. Position detection devices were installed in the first and last vehicles, and communication records were obtained using ground communication terminals approximately every 500 m. The measured track irregularities were converted from the time to distance functions using this communication record and train speed data. In addition, the position of the last vehicle relative to the first vehicle was finely corrected by cross-correlation of the measured data. The sampling of the acquisition system was 2 kHz and all data were converted into distance series response of 250 mm intervals. By applying the proposed method, the RDI was calculated from the obtained track irregularities, which included the bridge response of the first and last vehicles. By simultaneously referring to the calculated RDI and facility information, we detected few bridges with a high possibility of resonance issue.

All these processes were performed on the track maintenance management database system (called LABOCS). LABOCS is a de facto standard system for track maintenance and management in Japan, and it has already been in use for a long time by Japan's high-speed railways [55,56]. Fig. 20 shows a LABOCS display screen. For all high-speed railway lines in Japan, information on the ground facilities (including the bridges) were available on LABOCS. Therefore, by implementing the proposed method on LABOCS, it is possible to compute the track irregularity data and the RDI and comparing them with the structure's specifications. Although there are various types of bridges, such as steel, concrete, I-girder, and box girder, all bridges are displayed as truss-type objects in LABOCS.

4.2. Resonant bridge detection results

Fig. 21 shows (from top to bottom) the structure type, the structure span, the train speed, the track irregularities measured at the first and last vehicles, the filtered vehicle-length irregularities, the enveloped vehicle-length irregularity amplitudes, and the RDI. The train speed is ~ 230 km/h. The measured track irregularities are shown as 40-m mid-chord versine displacements used for track maintenance in Japan. There are six bridges from A1 to A6 in the section. The other section comprises bridges with rigid frames [71] that were frequently used in place of embankments in Japan's high-speed railways. The difference between the first and last vehicles is small except for the section of the bridge A3. On the bridge A3, the filtered

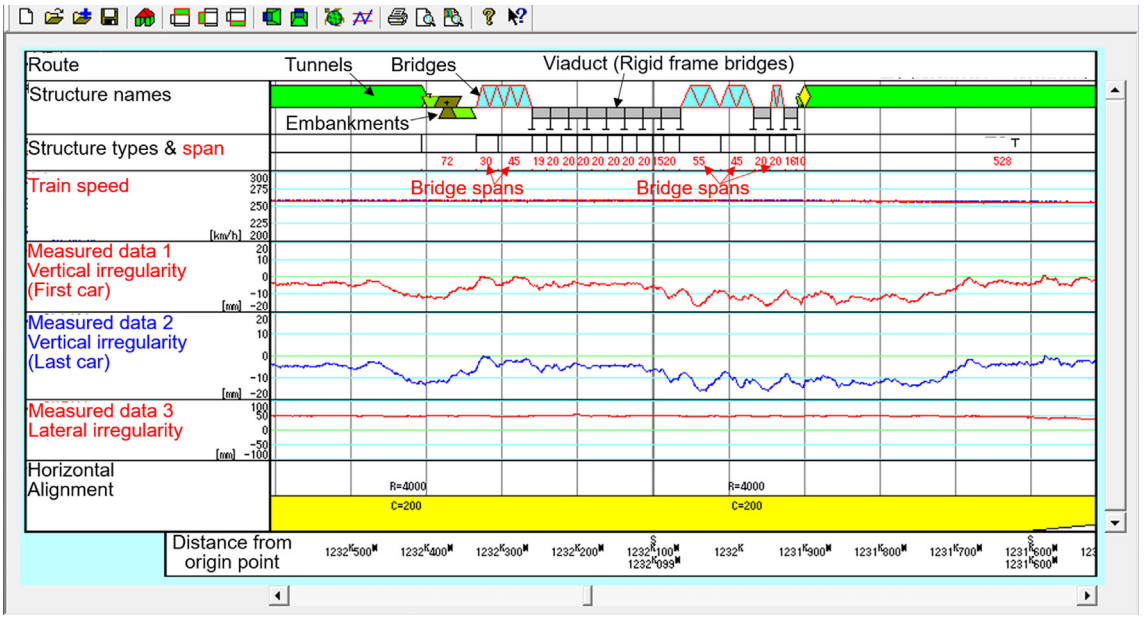

Fig. 20. Display screen of the track maintenance management database system LABOCS.

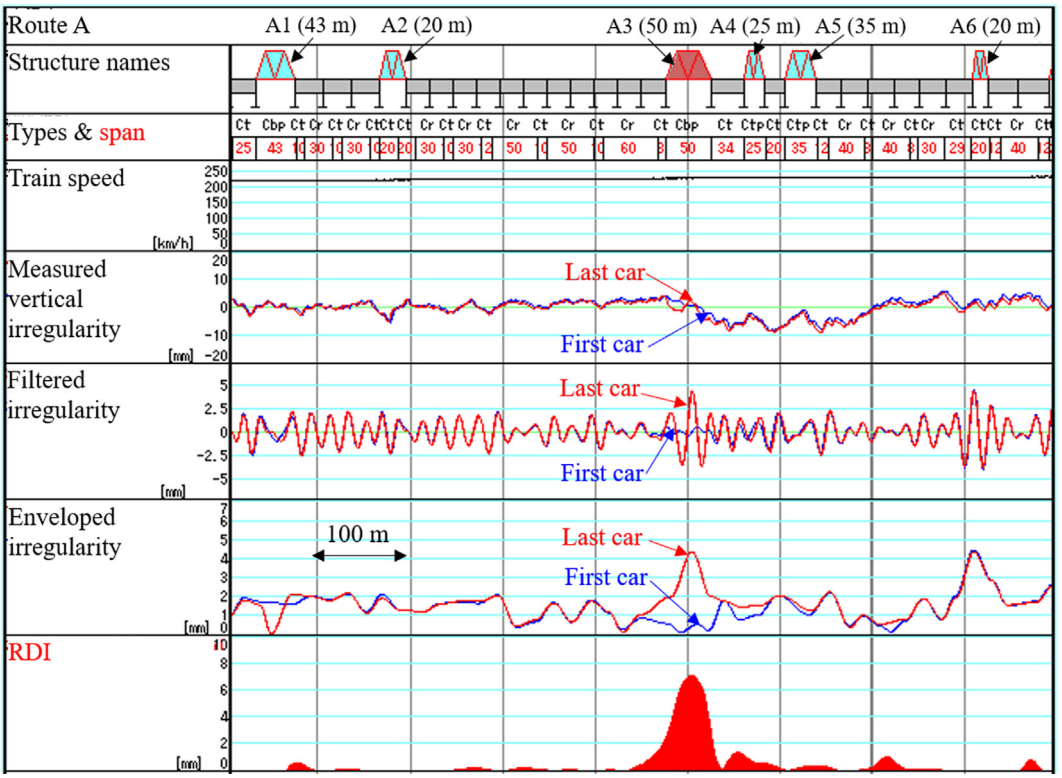

Fig. 21. Measured track irregularity and calculated RDI (section A).

vehicle length irregularity of the last vehicle is larger than that of the first vehicle. The enveloped vehicle length irregularity amplitude of the last vehicle in the bridge A3 section is larger than that of the first vehicle. Consequently, the RDI value shows a convex peak in which the dominant span almost coincides with the bridge A3 span. This tendency is almost consistent with numerical validations. Therefore, we assume that bridge A3 is in resonance with a train speed of 230 km/h

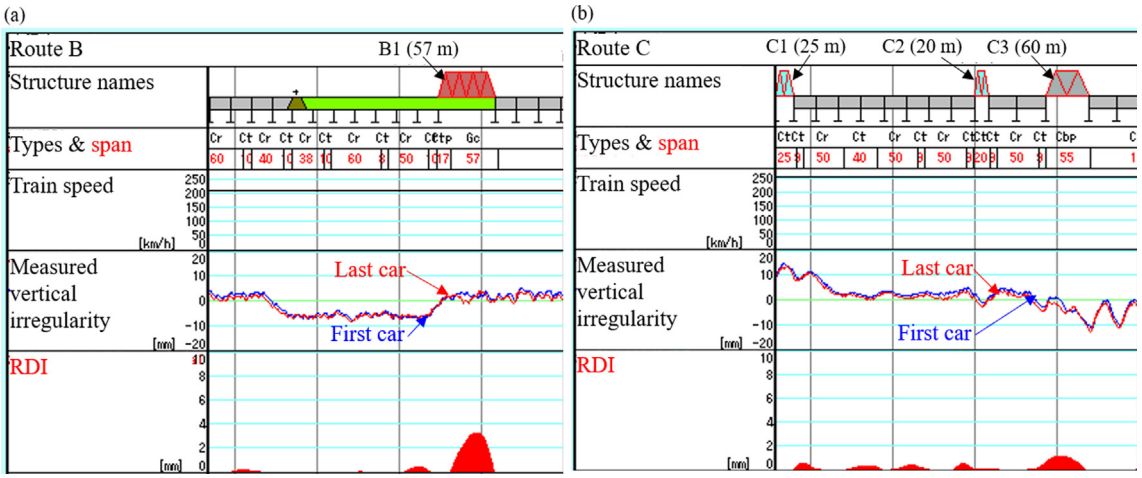

Fig. 22. Measured track irregularity and calculated RDI at (a) section B and (b) section C.

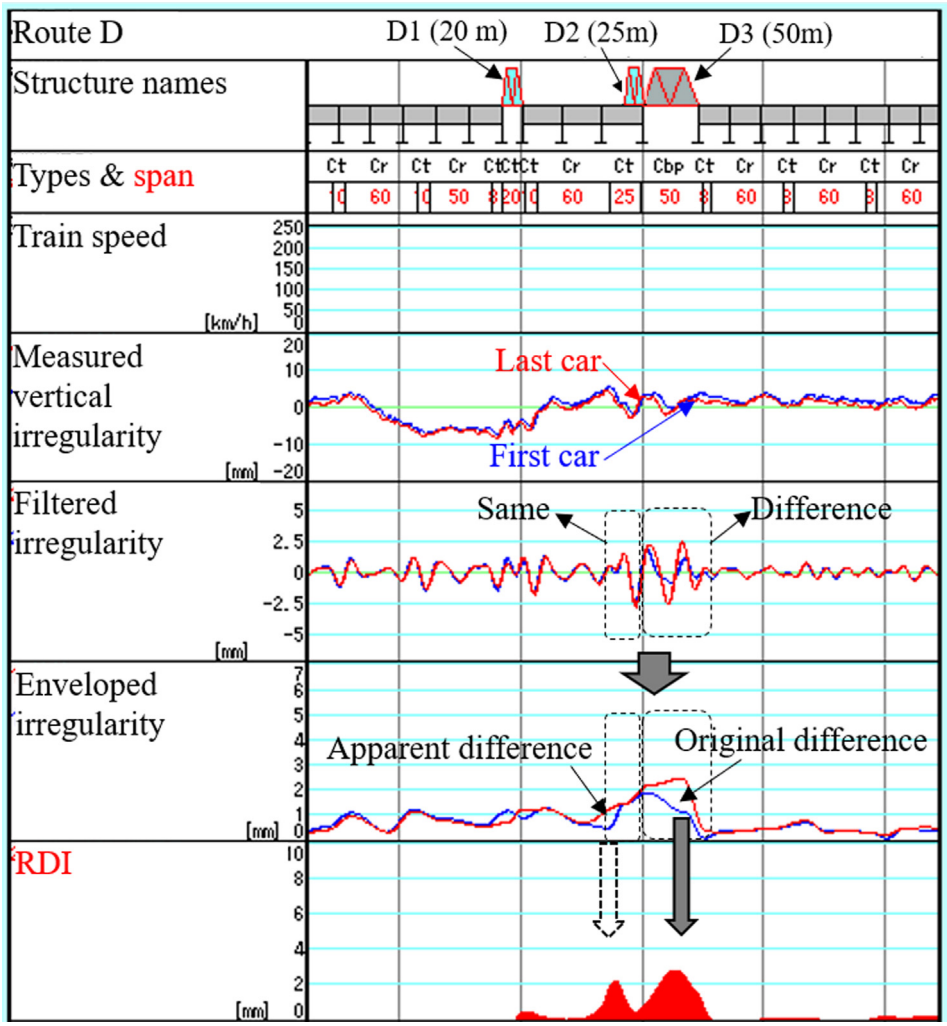

Fig. 23. Apparent RDI peak observed.

Table 2
Outline of target bridges.

ID	Girder type	Span (m)	Detection results by the drive-by method
A3	Concrete box	50	Resonance
C3	Concrete box	60	Beat (weak resonance)
D3	Concrete box	50	Resonance

and, as will be shown in Section 4.3, we verified whether this bridge actually resonates. For all other bridges and in case of rigid frame bridges, most RDIs are < 1 mm. Therefore, structures other than the bridge A3 are estimated to be non-resonant at a train speed of 230 km/h.

Fig. 22 shows the measured track irregularities and the calculated RDI values in the sections B and C as examples of the typical locations where the RDI features were identified. For a train traveling at the speed of 210 km/h in section B, it is possible to see RDI peaks that correspond to bridge B1, which has a span of 57 m. More than ten bridges with clear RDI peaks at the dominant wavelength coinciding with the bridge span, such as A3 and B1, could be observed along the target route. In section C, the train speed was 250 km/h. In the case of bridge C3, having a 60-m span, we could confirm the presence of a small component with a peak amount of ~ 1 mm having the same dominant wavelength as the bridge span. The possibility of false detection because of track irregularities without bridge displace component cannot be ignored because the number of RDI values is small. However, the RDI dominance in other sections was ~ 0.5 mm. Therefore, it was possible that the train speed was close to the resonance, and the beating phenomenon occurred.

Fig. 23 shows the measurement at section D where a particular trend of RDI can be observed. This section has three bridges from D1 to D3. According to RDI, we can assume that the bridges D2 and D3 with spans of 25 and 50 m, respectively, are resonant. However, although the difference between the first and last vehicles can be confirmed at the filtered vehicle length irregularities in the section of bridge D3, the filtered vehicle length irregularities of the first and last vehicles almost coincide in the bridge D2 section. However, the enveloped vehicle length irregularity amplitudes have a difference between the first and last vehicle in the bridge D2 section and the bridge D3 section. This indicates that apparent differences could occur in the case of adjacent bridges due to the influence of the dominant shape of the resonant bridge during envelope processing. In sections with continuous adjacent bridges, it is necessary to pay attention to the influence of resonant bridges on adjacent bridges. Even in such cases, it is possible to determine whether the RDI peak is apparent or true by comparing the filtered track irregularities of the first and last vehicles.

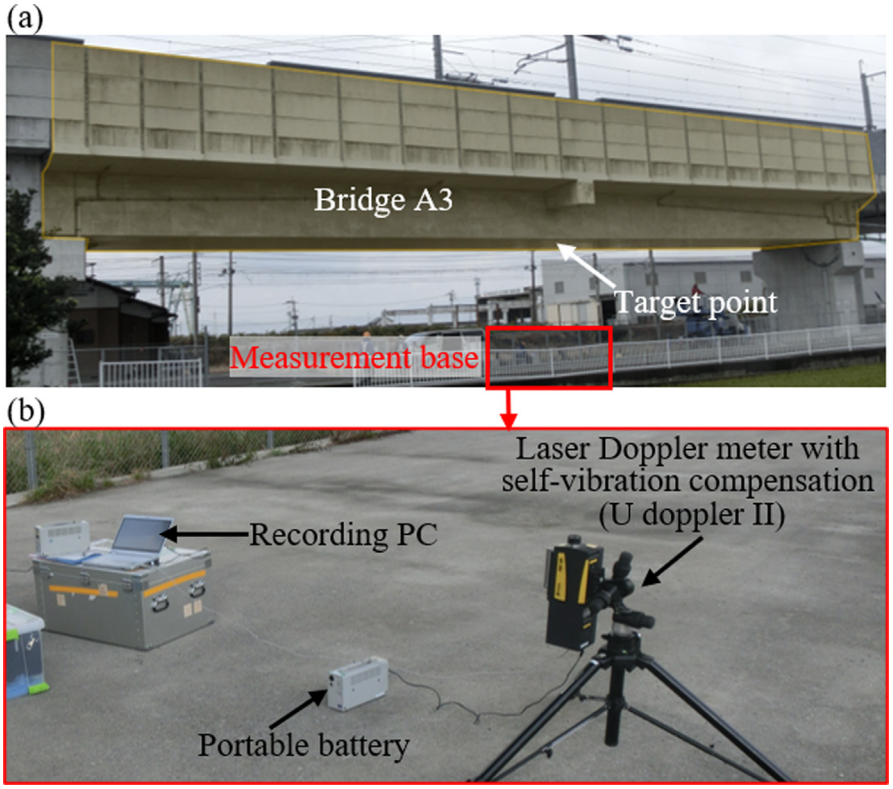

Fig. 24. Schematic of field test of the bridge A3 showing (a) the target bridge A3 and (b) the measuring device U Doppler II.

4.3. Verification of resonant bridge detection results

To confirm whether indications regarding the resonance bridges provided by the proposed method were correct, *in situ* measurements were performed on bridges A3, C3, and D3 mentioned above. All bridges comprise a prestressed concrete box girder and Table 2 reports the outline of the target bridges.

For bridges A3 and C3, the bridge response velocities under train passing were measured from below the bridge using a laser Doppler velocimeter with self-vibration compensation (U Doppler II, sampling 2000 Hz [72]). By integrating the obtained response velocity, we measured the vertical displacement of bridges when the trains passed over them. For the details of U Doppler II, see [72]. Fig. 24 shows the field measurements and the equipment used for A3 bridge. For bridge D3, located over a river, an accelerometer (MicroStone MVP-RE8-HC-2000, sampling 500 Hz) was installed on the bridge girder. In all cases, the objective was to measure the position of the bridge mid-span.

Fig. 25 shows the time-series responses of the bridges A3, C3, and D3 obtained by *in situ* measurements of bridges. In the case of bridges A3 and D3, the dynamic response amplitude of the bridge increases when the train passes over it. Furthermore, a large free vibration was observed after the passing of the train. This is the typical waveform of a resonant bridge passing through a train. Fig. 26 shows the maximum displacement of the bridge A3 at other train speeds. As shown in Fig. 26, the bridge A3 resonates with a peak maximum amplitude at the train speed of 225–230 km/h. Therefore, we confirmed that the resonant bridges could be detected by the proposed method.

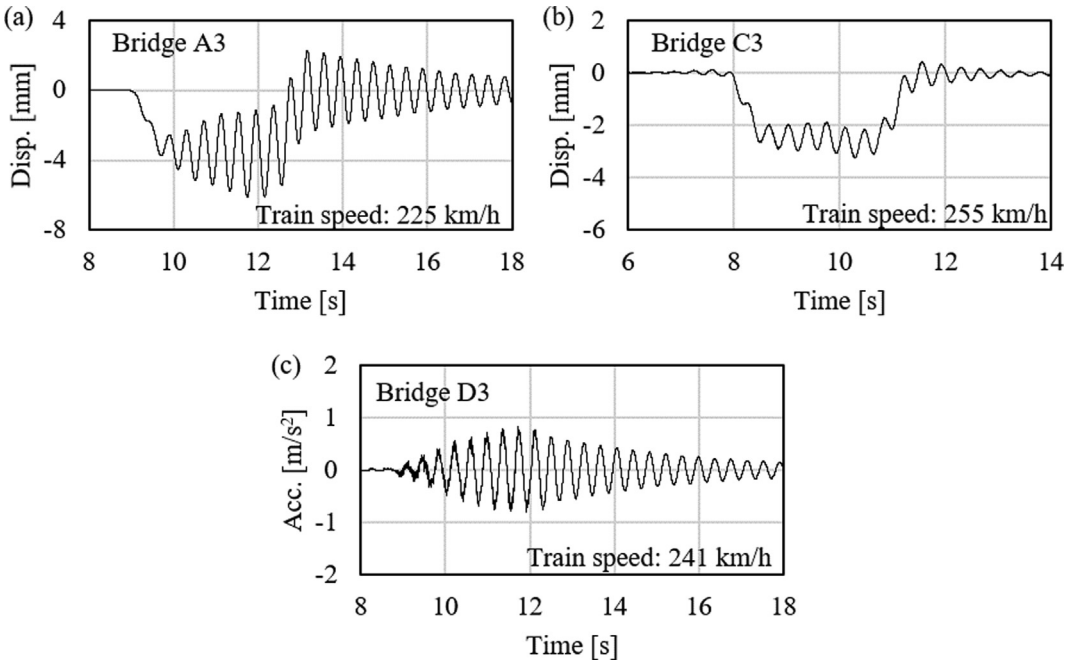

Fig. 25. In situ measured bridge responses: (a) Bridge A3, (b) Bridge C3, and (c) Bridge D3.

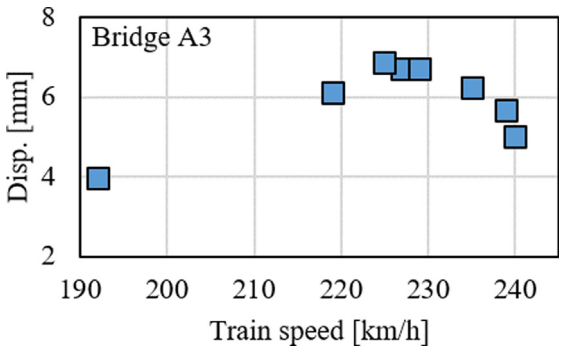

Fig. 26. Relationship between the maximum bridge displacement and train speed at the bridge A3.

The dynamic response amplitude of the bridge C3 shown in Fig. 25 (b) slightly increases when the train passes over it. This behavior it is not as pronounced as the dynamic response amplitude of the bridge A3; therefore, it is not completely resonant. However, the free vibration waveform can be seen after the train passes; therefore, the state of the bridge C3 was estimated as a beating state with weak resonance such that the train traveling speed slightly deviated from the resonance speed. As shown in Fig. 22 (b), it is possible to confirm that when the RDI peak is greater than 1 mm and the peak wavelength matches the bridge span, the bridge in the beat state can be detected. This fact shows the possibility of detecting a potential resonant bridge before it becomes completely resonant.

5. Conclusions

In this study, we developed a drive-by system able to detect resonant bridges from data measured using high-speed railway vehicles. A novel methodology to detect a resonant bridge was proposed, focusing on differences in track irregularities, including bridge displacement components measured using the first and last vehicles. Following numerical verification, the proposed method was applied to experimental data of track irregularities obtained from the high-speed railways of Japan and validated using *in situ* measurements. Using these analyses, we demonstrated that resonant bridges could be detected by the track maintenance management system that is already used daily by Japan's railway companies. Our results are summarized below.

(1) Using a bandpass filter and an envelope processing method to estimate the vehicle length track irregularity, it was possible to emphasize the unique components of the resonant bridge. In addition, a Resonance Detection Index (RDI) was defined using the difference between the filtered and enveloped track irregularities measured by the first and last vehicles. Through an appropriate methodology, RDI peaks and peak span can be used to detect resonant bridges.
(2) Using the parameter of bridge span, a numerical verification clarified that, although the maximum RDI value at resonance decreases as the span increases, resonant bridges with spans of 20–60 m can be estimated using the RDI.
(3) Measurement error, position synchronization error, and track irregularity were considered in the simulation. Signal noise and positioning error have a negligible effect, whereas RDI fluctuates by up to ± 2 mm due to the irregularity component with a wavelength that coincides with vehicle length. This variation could explain the misevaluation of resonance at a resonance speed of approximately –10 km/h if the bridge span is 50 m or more.
(4) The proposed method was applied to experimental data acquired by typical bogie-mounted track irregularity measurement devices installed on some trains in service on Japanese high-speed railways. More than ten resonant bridges were identified based on the RDI. Moreover, *in situ* bridge displacement measurements for three of these detected bridges demonstrated the utility of identification procedure.

Considering all of the above analyses, we clarified that measured rail profiles (i.e., track irregularities including bridge displacement) are different between the first and last vehicles in the case of resonant bridges; however, these differences can be used to identify resonant bridges. The proposed method can be introduced without any additional investment using track irregularity devices already installed and operative on the first and last vehicles of certain high-speed commercial trains in Japan. Furthermore, this research demonstrates that drive-by systems for bridges can be used at high speeds, and that the results can provide the basis for more sophisticated drive-by systems in future. Note that additional research is required in future to design a more general drive-by bridge inspection system.

Possible future developments could include:

Research on track type. In this study, we considered slab-type tracks with relatively strong and stable track conditions. However, the ballasted tracks that are frequently used in Europe exhibit variations in their physical properties and local settlements [46]. Therefore, it is possible that deformation of the track structure and bridge displacement components are more mixed in ballasted tracks. Although filtered track irregularities with wavelengths equal to the vehicle length are used to detect resonant bridges, track settlements that deform downward with a span of half a vehicle length can be confused with resonant bridge components. In future, it will be necessary to develop a separation method for these components.

Research on the availability of other sensors. A limited number of commercial vehicles are equipped with on-board track irregularity measurement devices. Data measured by general high-speed vehicles include bogie acceleration [50] for vehicle anomaly detection and carbody acceleration [73] for ride comfort management. Moreover, the development of resonant bridge detection methods using these sensors is effective for realizing more general drive-by systems in future. When developing these methods, it is necessary to solve problems such as the effect of the vehicle vibration state caused by adjacent bridges on the target bridge resonance in the case of multiple simply-supported bridges. However, knowledge obtained from this study could be used in such research.

CRediT authorship contribution statement

Kodai Matsuoka: Conceptualization, Methodology, Writing - original draft. **Hirofumi Tanaka:** Investigation, Writing - review & editing. **Kyohei Kawasaki:** Software, Validation, Visualization. **Claudio Somaschini:** Writing - review & editing, Validation. **Andrea Collina:** Methodology, Supervision.

Declaration of Competing Interest

The authors declare that they have no known competing financial interests or personal relationships that could have appeared to influence the work reported in this paper.

Acknowledgments

This study was conducted as a part of an international collaboration research project "Research on diagnostics method of bridges using the on-board measurement" between Politecnico di Milano, Department of Mechanical Engineering in Italy and the Railway Technical Research Institute in Japan.

Appendix A. Vehicle–bridge dynamic interaction model

In this appendix, we derive the motion equations of the vehicle–bridge dynamic interaction (hereinafter VBI) model shown in Fig. 27. The responses of the railway bridges and a train crossing at a constant speed v [m/s] were modeled on a two-dimensional simply-supported beam and a two-dimensional vehicle model with six degrees of freedom per vehicle. A similar model has been investigated in many previous studies [52,63,64]; therefore, we provide only an outline of this model here. The degrees of freedom of the bridge and vehicle are defined as the row vectors $\mathbf{Z}_{N,t} = [z_{1,t}, \cdots, z_{N,t}]^T$ and $\mathbf{Z}_{c,t} = [z_{c,t}, \psi_{c,t}, z_{t1,t}, \psi_{t1,t}, z_{t2,t}, \psi_{t2,t}]^T$, respectively. Let the wheelset freedoms $\mathbf{Z}_{w,t}$ be equal to the sum of the bridge displacement $\mathbf{Z}_{N,t}\mathbf{A}$ and the rail irregularity $\mathbf{r}$ at the axle position:

$$\mathbf{Z}_{w,t} = \mathbf{Z}_{N,t}\mathbf{A} + \mathbf{r} \tag{A.1}$$

The vehicle–bridge interaction model is defined by the following equation:

$$\begin{aligned} &\begin{bmatrix} \mathbf{M}_b^* & \\ & \mathbf{M}_c \end{bmatrix} \begin{bmatrix} \ddot{\mathbf{Z}}_{N,t} \\ \ddot{\mathbf{Z}}_{c,t} \end{bmatrix} + \begin{bmatrix} \mathbf{C}_b^* & \mathbf{C}_{b,c} \\ \mathbf{C}_{c,b} & \mathbf{C}_c \end{bmatrix} \begin{bmatrix} \dot{\mathbf{Z}}_{N,t} \\ \dot{\mathbf{Z}}_{c,t} \end{bmatrix} + \begin{bmatrix} \mathbf{K}_b^* & \mathbf{K}_{b,c} \\ \mathbf{K}_{c,b} & \mathbf{K}_c \end{bmatrix} \begin{bmatrix} \mathbf{Z}_{N,t} \\ \mathbf{Z}_{c,t} \end{bmatrix} \\ &= \begin{bmatrix} \mathbf{A}^T \left(\mathbf{F}_{gw} - \mathbf{K}_{wt}\mathbf{K}_{tt}^{-1}\mathbf{F}_{gt} \right) \\ 0 \end{bmatrix} - v^2 \begin{bmatrix} \mathbf{A}^T\mathbf{M}_w \\ 0 \end{bmatrix} \ddot{\mathbf{r}} - v \begin{bmatrix} \mathbf{A}^T\mathbf{C}_w \\ -\mathbf{C}_{tw} \end{bmatrix} \dot{\mathbf{r}} - \begin{bmatrix} \mathbf{A}^T\mathbf{K}_w \\ -\mathbf{K}_{tw} \end{bmatrix} \mathbf{r} \end{aligned} \tag{A.2}$$

where

$$\mathbf{M}_b^* = \mathbf{M}_b + \mathbf{A}^T\mathbf{M}_w\mathbf{A} \tag{A.3}$$

$$\mathbf{C}_b^* = \mathbf{C}_b + \mathbf{A}^T\mathbf{C}_w\mathbf{A}, \tag{A.4}$$

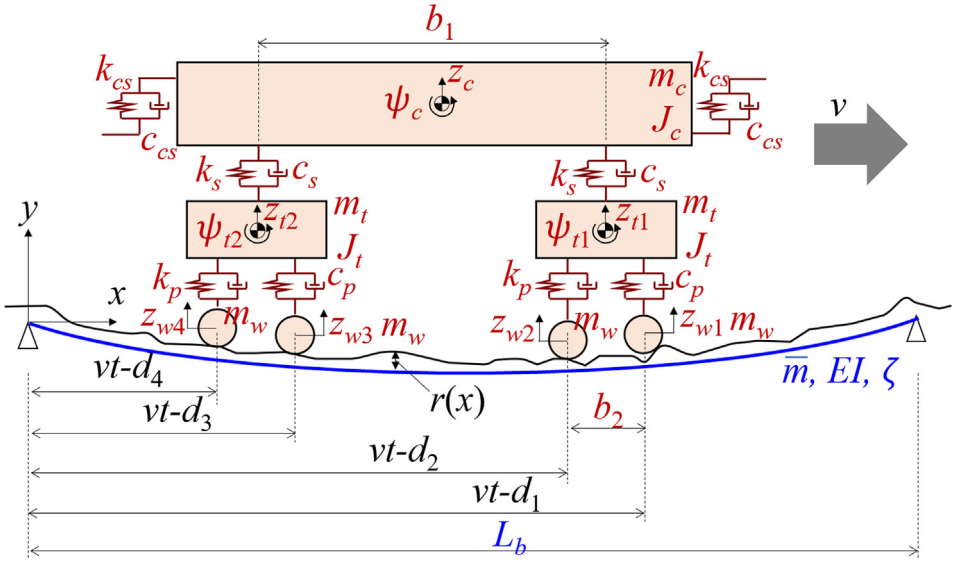

Fig. 27. Passage of a six degrees-of-freedom vehicle model on a simple-supported beam.

$$\mathbf{K}_b^* = \mathbf{K}_b + \mathbf{A}^T\mathbf{K}_w\mathbf{A} \tag{A.5}$$

$$\mathbf{A}(i,n) = \sin\left\{\frac{n\pi(vt-\tau_i)}{L_b}\right\}\left\{H\left(t-\frac{\tau_i}{v}\right) - H\left(t-\frac{\tau_i+L_b}{v}\right)\right\}$$

with

$$(i = 1,\cdots,nw), (n = 1,\cdots,N) \tag{A.6}$$

$$\mathbf{F}_{gw} = [-m_w g, -m_w g, -m_w g, -m_w g]^T \tag{A.7}$$

$$\mathbf{F}_{gt} = [-m_c g, 0, -m_t g, 0, -m_t g, 0]^T \tag{A.8}$$

$\mathbf{M}_b$, $\mathbf{C}_b$, and $\mathbf{K}_b$ are the mass, the damping, and the rigidity matrices, respectively, in the modal coordinates of the bridge. These matrices are expressed as follows:

$$\mathbf{M}_b = \mathrm{Diag}(m_{b1},\cdots,m_{bN}) = \mathrm{Diag}(\overline{m}L_b/2,\cdots,\overline{m}L_b/2), \tag{A.9}$$

$$\mathbf{C}_b = \mathrm{Diag}(c_{b1},\cdots,c_{bN}) = \mathrm{Diag}\left(2\xi_1\sqrt{m_{b1},k_{b1}},\cdots,2\xi_N\sqrt{m_{bN},k_{bN}}\right), \tag{A.10}$$

$$\mathbf{K}_b = \mathrm{Diag}(k_{b1},\cdots,k_{bN}) = \mathrm{Diag}\left((2\pi f_1)^2\overline{m},\cdots,\left(2\pi N^2 f_N\right)^2\overline{m}\right). \tag{A.11}$$

$\mathbf{M}_c$, $\mathbf{C}_c$, and $\mathbf{K}_c$ are the mass, the damping, and rigidity matrices, respectively, of the vehicle. $\mathbf{M}_w$, $\mathbf{C}_w$, and $\mathbf{K}_w$ are the mass, the damping, and the rigidity matrices, respectively, of the wheelsets. $\mathbf{C}_{b,c}$ ($\mathbf{C}_{c,b} = \mathbf{C}_{b,c}^T$) and $\mathbf{K}_{b,c}$ ($\mathbf{K}_{c,b} = \mathbf{K}_{b,c}^T$) are the coupling terms related to the vehicle dampers and springs, respectively:

$$\mathbf{M}_c = \mathrm{Diag}(m_c, J_c, m_t, J_t, m_t, J_t) \tag{A.12}$$

$$\mathbf{C}_c = \begin{bmatrix} 2c_s & 0 & -c_s & 0 & -c_s & 0 \\ & \frac{c_s b_1^2}{2} & \frac{c_s b_1}{2} & 0 & -\frac{c_s b_1}{2} & 0 \\ & & c_s + 2c_p & 0 & 0 & 0 \\ & & & \frac{c_p b_2^2}{2} & 0 & 0 \\ & Sym. & & & c_s + 2c_p & 0 \\ & & & & & \frac{c_p b_2^2}{2} \end{bmatrix} \tag{A.13}$$

$$\mathbf{K}_c = \begin{bmatrix} 2k_s & 0 & -k_s & 0 & -k_s & 0 \\ & \frac{k_s b_1^2}{2} & \frac{k_s b_1}{2} & 0 & -\frac{k_s b_1}{2} & 0 \\ & & k_s + 2k_p & 0 & 0 & 0 \\ & & & \frac{k_p b_2^2}{2} & 0 & 0 \\ & Sym. & & & k_s + 2k_p & 0 \\ & & & & & \frac{k_p b_2^2}{2} \end{bmatrix} \tag{A.14}$$

$$\mathbf{M}_w = \mathrm{diag}(m_w, m_w, m_w, m_w), \tag{A.15}$$

$$\mathbf{C}_w = \mathrm{diag}(c_p, c_p, c_p, c_p) \tag{A.16}$$

$$\mathbf{K}_w = \mathrm{diag}(k_p, k_p, k_p, k_p) \tag{A.17}$$

$$\mathbf{C}_{b,c} = \begin{bmatrix} 0 & 0 & -c_p & -\frac{c_p b_2}{2} & 0 & 0 \\ 0 & 0 & -c_p & -\frac{c_p b_2}{2} & 0 & 0 \\ 0 & 0 & 0 & 0 & -c_p & -\frac{c_p b_2}{2} \\ 0 & 0 & 0 & 0 & -c_p & -\frac{c_p b_2}{2} \end{bmatrix} \tag{A.18}$$

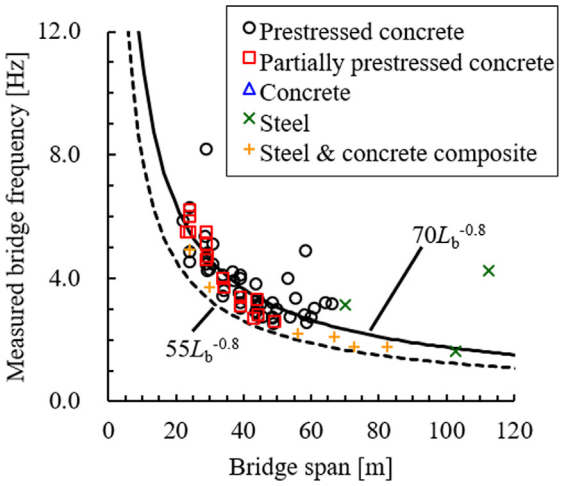

Fig. 28. Relationship between the bridge fundamental frequency and the span (Japan's high-speed railway bridges).

$$\mathbf{K}_{b,c} = \begin{bmatrix} 0 & 0 & -k_p & -\frac{k_p b_2}{2} & 0 & 0 \\ 0 & 0 & -k_p & -\frac{k_p b_2}{2} & 0 & 0 \\ 0 & 0 & 0 & 0 & -k_p & -\frac{k_p b_2}{2} \\ 0 & 0 & 0 & 0 & -k_p & -\frac{k_p b_2}{2} \end{bmatrix} \tag{A.19}$$

The vehicles are coupled through the vertical spring k_{cs} and the damper c_{cs}. These components are introduced into the coupling term of the vertical displacement and the rotational degrees of freedom of the car bodies of two adjacent vehicles (when the vehicle model contains two or more cars).

The VBI model (A.2) was solved and modeled in state space. Numerical integration was performed by the explicit Runge–Kutta method [4, 5] proposed by Dormand and Prince (also known as RK5(4)7FM, DOPRI5, and DP(4, 5) [74]). The present VBI model simulation considers the bridge modes 1–3 (i.e., N = 3) [52].

Appendix B. Bridge span–frequency relationship in Japan

Fig. 28 shows the relationship between the bridge fundamental frequency and the span. These results were estimated by the Fourier transform of the free vibration responses after the train passed; the displacements were measured for Japan's high-speed railways. It can be confirmed that the measured lower limit of the bridge fundamental frequency of the bridge corresponds to approximately $55L_b^{-0.8}$.

References

[1] T. Asada, C. Roberts, T. Koseki, An algorithm for improved performance of railway condition monitoring equipment: alternating-current point machine case study, Transp. Res. C 30 (2013) 81–92, https://doi.org/10.1016/j.trc.2013.01.008.
[2] Junki Nakasuka, T. Mizutani, Y. Yamamoto, M. Uchida, T.N. Di Su, Y. Fujino, Analysis of large amplitude vibration mechanism of Shinkansen PRC girder bridges and the long-term trend of their structural characteristics, J. Struct. Eng., A 62A (2016) 42–49, Released April 24, 2017, (In Japanese).
[3] M. Sogabe, N. Matsumoto, M. Kanamori, H. Wakui, Impact factors of concrete girders coping with train speed-up, Quarterly Re-port of RTRI 46 (2005) 46–52.
[4] K. Matsuoka, M. Tokunaga, D. Tsukishima, K. Goto. Dynamic Response Evaluation of Resonance PRC Girder with Additional Reinforcement Supports, JCI Annual Convention Proceedings Vol. 41 (pp. 1219–1224), 2019. (In Japanese).
[5] S. Shinozaki, K. Matsuoka, K. Kaito. Bayesian Analysis for the Effect of Uncertainty about Bridge Strength in Reinforcement by Additional Support, JCI Annual Convention Proceedings Vol. 41 (pp. 1399–1404), 2019. (In Japanese).
[6] Eurocode 1: Actions on structures – Part2. Traffic Loads on Bridges. European Committee for Standardization, 1991
[7] Y. Ogiwara, T. Shinada, S. Harada. Countermeasure Construction for the Resonance of the PRC Girder in the Hokuriku Shinkansen, JCI Annual Convention Proceedings Vol. 41 (pp. 1441–1446), 2019. (In Japanese).
[8] O.S. Salawu, Detection of structural damage through changes in frequency: a review, Eng. Struct. 19 (1997) 718–723, https://doi.org/10.1016/S0141-0296(96)00149-6.
[9] Z. Wu, Y. Fujino, Structural health monitoring and intelligent infrastructure, Smart Mater. Struct. 14 (2005).
[10] A. Bellino, A. Fasana, L. Garibaldi, S. Marchesiello, PCA-based detection of damage in time-varying systems, Mech. Syst. Signal Process. 24 (2010) 2250–2260, https://doi.org/10.1016/j.ymssp.2010.04.009.
[11] X.W. Ye, Y.H. Su, J.P. Han, Structural health monitoring of civil infrastructure using optical fiber sensing technology: A comprehensive review, ScientificWorldJournal 2014 (2014), https://doi.org/10.1155/2014/652329, Pubmed:25133250.
[12] D. Feng, M.Q. Feng, Experimental validation of cost-effective vision-based structural health monitoring, Mech. Syst. Signal Process. 88 (2017) 199–211, https://doi.org/10.1016/j.ymssp.2016.11.021.

[13] D. Hester, A. González, A discussion on the merits and limitations of using drive-by monitoring to detect localised damage in a bridge, Mech. Syst. Signal Process. 90 (2017) 234–253, https://doi.org/10.1016/j.ymssp.2016.12.012.
[14] Y.B. Yang, J.P. Yang, Y. Wu, B. Zhang. Vehicle Scanning Method for Bridges, 2019
[15] Y.-B. Yang, C.W. Lin, J.D. Yau, Extracting bridge frequencies from the dynamic response of a passing vehicle, J. Sound Vib. 272 (2004) 471–493, https://doi.org/10.1016/S0022-460X(03)00378-X.
[16] C.W. Lin, Y.B. Yang, Use of a passing vehicle to scan the fundamental bridge frequencies: an experimental verification, Eng. Struct. 27 (2005) 1865–1878, https://doi.org/10.1016/j.engstruct.2005.06.016.
[17] Y.B. Yang, K.C. Chang, Extracting the bridge frequencies indirectly from a passing vehicle: parametric study, Eng. Struct. 31 (2009) 2448–2459, https://doi.org/10.1016/j.engstruct.2009.06.001.
[18] Y.B. Yang, K.C. Chang, Y.C. Li, Filtering techniques for extracting bridge frequencies from a test vehicle moving over the bridge, Eng. Struct. 48 (2013) 353–362, https://doi.org/10.1016/j.engstruct.2012.09.025.
[19] Y.B. Yang, Z.L. Wang, K. Shi, H. Xu, Y.T. Wu, State-of-the-art of the vehicle-based methods for detecting the various properties of highway bridges and railway tracks, Int. J. Struct. Stab. Dyn. (2020) 2041004, https://doi.org/10.1142/S0219455420410047.
[20] F. Cerda, S. Chen, J. Bielak, J.H. Garrett, P. Rizzo, J. Kovacevic, Indirect structural health monitoring of a simplified laboratory-scale bridge model, Smart Struct. Syst. 13 (2014) 849–868, https://doi.org/10.12989/sss.2014.13.5.849.
[21] K.C. Chang, C.W. Kim, M. Kawatani, Feasibility investigation for a bridge damage identification method through moving vehicle laboratory experiment, Struct. Infrastruct. Eng. 10 (2014) 328–345, https://doi.org/10.1080/15732479.2012.754773.
[22] C.W. Kim, R. Isemoto, P.J. McGetrick, M. Kawatani, E.J. O'Brien, Drive-by bridge inspection from three different approaches, Smart Struct. Syst. 13 (2014) 775–796. 10.12989/sss.2014.13.5.775.
[23] P.J. McGetrick, C.W. Kim, A. González, E.J.O. Brien, Experimental validation of a drive-by stiffness identification method for bridge monitoring, Struct. Health Monit. 14 (2015) 317–331, https://doi.org/10.1177/1475921715578314.
[24] C.W. Kim, R. Isemoto, T. Toshinami, M. Kawatani, P. McGetrick, E.J. O'Brien, Experimental investigation of drive-by bridge inspection, in: 5th International Conference on Structural Health Monitoring of Intelligent Infrastructure (SHMII-5), Cancun, Mexico, December 11–15, 2011. Instituto de Ingeniería, UNAM, 2011.
[25] A. Elhattab, N. Uddin, E. OBrien, Drive-by bridge damage monitoring using Bridge Displacement Profile Difference, J. Civ. Struct. Health Monit. 6 (2016) 839–850. 10.1007/s13349-016-0203-6
[26] W. Locke, J. Sybrandt, L. Redmond, I. Safro, S. Atamturktur, Using drive-by health monitoring to detect bridge damage considering environmental and operational effects, J. Sound Vib. 468 (2020), https://doi.org/10.1016/j.jsv.2019.115088, 115088.
[27] A. Elhattab, N. Uddin, E. OBrien, Drive-by bridge frequency identification under operational roadway speeds employing frequency independent underdamped pinning stochastic resonance (fi-upsr), Sensors 18 (2018) 4207. 10.3390/s18124207, Pubmed:30513669
[28] H. Wang, T. Nagayama, J. Nakasuka, B. Zhao, D. Su, Extraction of bridge fundamental frequency from estimated vehicle excitation through a particle filter approach, J. Sound Vib. 428 (2018) 44–58, https://doi.org/10.1016/j.jsv.2018.04.030.
[29] T. Nagayama, A.P. Reksowardojo, D. Su, T. Mizutani, Bridge natural frequency estimation by extracting the common vibration component from the responses of two vehicles, Eng. Struct. 150 (2017) 821–829, https://doi.org/10.1016/j.engstruct.2017.07.040.
[30] C.W. Kim, R. Isemoto, T. Toshinami, M. Kawatani, P.J. McGetrick, E.J. OBrien, Experimental investigation of drive-by inspection, in: 5th International Conference on Structural Health Monitoring of Intelligent Infrastructure (SHMII-5)2011: Cancun, Mexico, 2011.
[31] A. González, E.J. OBrien, P.J. McGetrick, Identification of damping in a bridge using a moving instrumented vehicle, J. Sound Vib. 331 (2012) 4115–4131. 10.1016/j.jsv.2012.04.019
[32]] J. Keenahan, E.J. OBrien, P.J. McGetrick, A. Gonzalez, The use of a dynamic truck–trailer drive-by system to monitor bridge damping, Struct. Health Monit. 13 (2014) 143–157. 10.1177/1475921713513974
[33] Y. Oshima, K. Yamamoto, K. Sugiura, Damage assessment of a bridge based on mode shapes estimated by responses of passing vehicles, Smart Struct. Syst. 13 (2014) 731–753, https://doi.org/10.12989/sss.2014.13.5.731.
[34] E.J. O'Brien, P.J. McGetrick, A. González, A drive-by inspection system via vehicle moving force identification, Smart Struct. Syst. 13 (2014) 821–848, https://doi.org/10.12989/sss.2014.13.5.821.
[35] K.V. Nguyen, H.T. Tran, Multi-cracks detection of a beam-like structure based on the on-vehicle vibration signal and wavelet analysis, J. Sound Vib. 329 (2010) 4455–4465, https://doi.org/10.1016/j.jsv.2010.05.005.
[36] Y. Zhang, S.T. Lie, Z. Xiang, Damage detection method based on operating deflection shape curvature extracted from dynamic response of a passing vehicle, Mech. Syst. Signal Process. 35 (2013) 238–254, https://doi.org/10.1016/j.ymssp.2012.10.002.
[37] S.L. Grassie, Measurement of railhead longitudinal profiles: a comparison of different techniques, Wear 191 (1996) 245–251, https://doi.org/10.1016/0043-1648(95)06732-9.
[38] P.F. Weston, C.S. Ling, C.J. Goodman, C. Roberts, P. Li, R.M. Goodall, Monitoring lateral track irregularity from in-service railway vehicles, Proc. Inst. Mech. Eng. F 221 (2007) 89–100, https://doi.org/10.1243/0954409JRRT64.
[39] M. Odashima, S. Azami, Y. Naganuma, H. Mori, H. Tsunashima, Track geometry estimation of a conventional railway from car-body acceleration measurement, Mech. Eng. J. 4 (2017) 16–00498, https://doi.org/10.1299/mej.16-00498.
[40] X. Wei, F. Liu, L. Jia, Urban rail track condition monitoring based on in-service vehicle acceleration measurements, Measurement 80 (2016) 217–228, https://doi.org/10.1016/j.measurement.2015.11.033.
[41] J. Real, P. Salvador, L. Montalbán, M. Bueno, Determination of rail vertical profile through inertial methods, Proc. Inst. Mech. Eng. F 225 (2011) 14–23, https://doi.org/10.1243/09544097JRRT353.
[42] J.I. Real Herráiz, M.L. Montalban Domingo, T. Real, V. Puig, Development of a system to obtain vertical track geometry measuring axle-box accelerations from in-service trains, J. Vibroengineering 14 (2012) 813–826.
[43] A. De Rosa, S. Alfi, S. Bruni, Estimation of lateral and cross alignment in a railway track based on vehicle dynamics measurements, Mech. Syst. Signal Process. 116 (2019) 606–623, https://doi.org/10.1016/j.ymssp.2018.06.041.
[44] Y.B. Yang, Z.L. Wang, K. Shi, H. Xu, X.Q. Mo, Y.T. Wu, Two-axle test vehicle for damage detection for railway tracks modeled as simply supported beams with elastic foundation, Eng. Struct. 219 (2020), https://doi.org/10.1016/j.engstruct.2020.110908.
[45] E. Yazawa, K. Takeshita, Development of measurement device of track irregularity using inertial mid-chord offset method, Quarterly Report of RTRI 43 (2002) 125–130.
[46] P. Quirke, D. Cantero, E.J. OBrien, C. Bowe, Drive-by detection of railway track stiffness variation using in-service vehicles, Proc. Inst. Mech. Eng. F 231 (2017) 498–514. https://doi.org/10.1177/0954409716634752
[47] A.H. Eslami-Khouzani, C. Caprani (2018, January), Potential of drive-by inspection for railway bridges, in: International Conference on Bridge Maintenance, Safety and Management (IABMAS). CRC Press, 2018 (pp. 945–952).
[48] K. Matsuoka, K. Kaito, M. Tokunaga, T. Watanabe, M. Sogabe, Identification of the vibration properties of bridge using the axle acceleration response of a running train. Journal of Japan Society of Civil Engineers, (Constr. Manag.), 68 F4 (2012) 175–192.(In Japanese).
[49] M. Carnevale, A. Collina, T. Peirlinck, A feasibility study of the drive-by method for damage detection in railway bridges, Appl. Sci. 9 (2019) 160, https://doi.org/10.3390/app9010160.
[50] C. Somaschini, M. Carnevale, K. Matsuoka, A. Collina, Damage detection in railway bridges by means of train on-board sensors, in: 12th World Congress on Railway Research, 2019 (pp. 1–6).
[51] H. Ouyang, Moving-load dynamic problems: a tutorial (with a brief overview), Mech. Syst. Signal Process. 25 (2011) 2039–2060, https://doi.org/10.1016/j.ymssp.2010.12.010.

[52] K. Matsuoka, K. Kaito, M. Sogabe, Bayesian time–frequency analysis of the vehicle–bridge dynamic interaction effect on simple-supported resonant railway bridges, Mech. Syst. Signal Process. 135 (2020), https://doi.org/10.1016/j.ymssp.2019.106373, 106373.
[53] L. Frýba. Vibration of Solids and Structures under Moving Loads Vol. 1. Springer Science & Business Media, 2013.
[54] Y. Tsubokawa, H. Tanaka, K. Hamaoka, H. Sato, Accuracy validation method and verification results of track measuring device with the inrtial mid chord offset method, Railway Engineering-2017. 10.25084/raileng.2017.0058, Railway Engineering, Engineering. Technics Press, Edinburgh
[55] A. Yoshimura, Y. Yoshida, M. Kamiyama, Development of database system for railway track maintenance management, Micro LABOCS for Windows and its features. Railway Technical Research Institute, Q. Rep. 38 (1997).
[56] Y. Tsubokawa, H. Tanaka, Commercial trains check tracks daily to collect data for maintenance planning, Ascent, 5 (2018) 9-14
[57] M.D. Martínez-Rodrigo, J. Lavado, P. Museros, Dynamic performance of existing high-speed railway bridges under resonant conditions retrofitted with fluid viscous dampers, Eng. Struct. 32 (2010) 808–828, https://doi.org/10.1016/j.engstruct.2009.12.008.
[58] J. Lavado, A. Doménech, M.D. Martínez-Rodrigo, Dynamic performance of existing high-speed railway bridges under resonant conditions following a retrofit with fluid viscous dampers supported on clamped auxiliary beams, Eng. Struct. 59 (2014) 355–374, https://doi.org/10.1016/j.engstruct.2013.10.038.
[59] J.M. Goicolea, J. Domínguez, J.A. Navarro, F. Gabaldón. New Dynamic Analysis Methods for Railway Bridges in Codes IAPF and Eurocode 1. Computational Mechanics Publications Group, Escuela Técnica Superior de Ingenieros de Caminos, Universidad Politécnica de Madrid, 2002
[60] C.R. Hendy, D.A. Smith (2007), Designers' guide to EN 1992–EN 1992: Eurocode 2: Design of Concrete Structures Part 2. Concrete. Thomas Telford, Bridges
[61] H. Xia, N. Zhang, W.W. Guo, Analysis of resonance mechanism and conditions of train–bridge system, J. Sound Vib. 297 (2006) 810–822, https://doi.org/10.1016/j.jsv.2006.04.022.
[62] A. Wiriyachai, K.H. Chu, V.K. Garg, Bridge impact due to wheel and track irregularities, J. Eng. Mech. Div. 108 (1982) 648–666.
[63] A. Matsuura. Dynamic Behavior of Bridge Girder for High Speed Railway Bridge, Quarterly Report of RTRI (pp. 70–76), 1979.
[64] A. Doménech, P. Museros, M.D. Martínez-Rodrigo, Influence of the vehicle model on the prediction of the maximum bending response of simply-supported bridges under high-speed railway traffic, Eng. Struct. 72 (2014) 123–139, https://doi.org/10.1016/j.engstruct.2014.04.037.
[65] M. Sogabe, A. Furukawa, T. Shimomura, T. Iida, N. Matsumoto, H. Wakui, Deflection limits of structures for train speed-up, Quarterly Report of RTRI 46 (2005) 130–136.
[66] Y.W. Zhang, J.H. Lin, Y. Zhao, W.P. Howson, F.W. Williams, Symplectic random vibration analysis of a vehicle moving on an infinitely long periodic track, J. Sound Vib. 329 (2010) 4440–4454, https://doi.org/10.1016/j.jsv.2010.05.004.
[67] X. Lei, N.-A. Noda, Analyses of dynamic response of vehicle and track coupling system with random irregularity of track vertical profile, J. Sound Vib. 258 (2002) 147–165, https://doi.org/10.1006/jsvi.2002.5107.
[68] H. Takai, M. Uchida, K. Takeshita, Y. Sunaga, Track maintenance technique for 300 km/h class Shinkansen, Railway Technical Research Institute, Q. Rep. 34 (1993).
[69] H. Tanaka, M. Matsumoto, M. Miwa, Y. Miyazaki, Comparison analysis of various evaluation indexes of track irregularity data for high-speed railway track, Railway Engineering-2017. 10.25084/raileng.2017.0021, Railway Engineering, Engineering. Technics Press, Edinburgh.
[70] H. Tanaka, S. Yamamoto, T. Oshima, M. Miwa, Methods for detecting and predicting localized rapid deterioration of track irregularity based on data measured with high frequency, Quarterly report of RTRI 59 (2018) 169–175.
[71] S. Nakamura, Y. Momiyama, T. Hosaka, K. Homma, New technologies of steel/concrete composite bridges, J. Constr. Steel Res. 58 (2002) 99–130, https://doi.org/10.1016/S0143-974X(01)00030-X.
[72] F. Uehan, Development of the U-Doppler non-contact vibration measuring system for diagnosis of railway structures, Quarterly Report of RTRI 49 (2008) 178–183.
[73] H. Tsunashima, Condition monitoring of railway tracks from car-body vibration using a machine learning technique, Appl. Sci. 9 (2019) 2734, https://doi.org/10.3390/app9132734.
[74] L.F. Shampine, M.W. Reichelt, The MATLAB ode suite, SIAM J. Sci. Comput. 18 (1997) 1–22, https://doi.org/10.1137/S1064827594276424.